

The Use of Equalization Filters to Achieve High Common Mode Rejection Ratios in Biopotential Amplifier Arrays

by

Hongfang Xia

A Thesis

Submitted to the Faculty

of

WORCESTER POLYTECHNIC INSTITUTE

in partial fulfillment of the requirements for the

Degree of Master of Science

in

Electrical and Computer Engineering

January 2005

APPROVED:

Professor Edward A. Clancy, Thesis Advisor

Professor Donald R. Brown, Committee Member

Professor Brian M. King, Committee Member

ACKNOWLEDGEMENTS

I would like to acknowledge my indebtedness to my advisor Professor Edward A. Clancy for his generous help and encouragement. I owed a lot to him, not just my engineering skills and knowledge. Without his support, I cannot finish my thesis and make these achievements with my research.

I am also thankful to Professor Brown for his helpful suggestions during my graduate study and his presence in the committee. I am also thankful to Professor Brian M. King for his presence in the committee, and all my friends, especially those in $C(SP)^2$ lab, including Mark, Karthik and Oli, who have gave me a lot of help in many ways.

I think I cannot give enough thanks to my dear family, especially my parents and my husband.

ABSTRACT

Recently, it became possible to detect single motor units (MUs) noninvasively via the use of spatial filtering electrode arrays. With these arrays, weighted combinations of monopolar electrode signals recorded from the skin surface provide spatial selectivity of the underlying electrical activity. Common spatial filters include the bipolar electrode, the longitude double differentiating (LDD) filter and the normal double differentiating (NDD) filter. In general, the spatial filtering is implemented in hardware and the performance of the spatial filtering apparatus is measured by its common mode rejection ratio (CMRR). High precision hardware differential amplifiers are used to perform the channel weighting in order to achieve high CMRR. But, this hardware is expensive and all channel weightings must be predetermined. Hence, only a few spatially filtered channels are typically derived.

In this project, a distinct software equalization filter was cascaded with each of the hardware monopolar signal conditioning circuits to achieve accurate weighting and high CMRR. The simplest technique we explored was to design an equalization filter by dividing the frequency response of a “reference” (or “ideal”) channel by the measured frequency response of the channel being equalized, producing the desired equalization filter in the frequency domain (conventional technique). Simulation and experimental results showed that the conventional technique is very sensitive to broadband background noise, producing poor CMRR. Thus, a technique for signal denoising that is based on signal mixing was pursued and evaluated both in simulation and laboratory experiments. The purpose of the mixing technique is to eliminate the noise as much as possible prior to equalization filter design. The simulation results show that without software equalization,

CMRR is only around 30 dB; with conventional technique CMRR is around 50~60 dB.

By using mixing technique, CMRR can be around 70~80 dB.

TABLE OF CONTENTS

ACKNOWLEDGEMENTS.....	- 1 -
ABSTRACT.....	- 2 -
TABLE OF CONTENTS.....	- 4 -
LIST OF TABLES.....	- 6 -
LIST OF FIGURES.....	- 7 -
CHAPTER 1 INTRODUCTION.....	- 1 -
1.1 Project Objectives.....	- 1 -
1.2 Thesis Outline.....	- 2 -
CHAPTER 2 BACKGROUND.....	- 4 -
2.1 EMG Introduction.....	- 4 -
2.2 Standard EMG Array Detection System.....	- 6 -
2.3 Common Mode Rejection Ratio (CMRR).....	- 13 -
2.3.1 Definition.....	- 13 -
2.3.2 Measurement of CMRR.....	- 14 -
CHAPTER 3 Simulation of Equalization Filters.....	- 17 -
3.1 Conventional technique.....	- 20 -
3.1.1 Equalization Filter Frequency Response.....	- 20 -
3.1.2 CMRR Measurement.....	- 22 -
3.1.3 Simulation Results For The Conventional Technique.....	- 26 -
3.2 Mixing Technique.....	- 30 -
3.2.1 Mixing Algorithm.....	- 31 -
3.2.2 System Configuration.....	- 35 -

3.2.3 CMRR Measurement	- 36 -
3.2.4 Simulation Results Using Mixing Technique	- 45 -
CHAPTER 4 LABORATORY EXPERIMENTS.....	- 48 -
4.1 Hardware Introduction	- 48 -
4.2 Experiment Results	- 54 -
4.2.1 Equalization Filter Response	- 54 -
4.2.2 CMRR Results	- 55 -
CHAPTER 5 PRELIMINARY RESULTS From A 28-CHANNEL ELECTRODE ARRAY	- 56 -
5.1 EMG hardware system.....	- 56 -
5.1.1 The EMG Array	- 56 -
5.1.2 Signal Conditional Circuits.....	- 58 -
5.2 Experiment Results	- 58 -
CHAPTER 6 CONCLUSIONS AND FUTURE WORK.....	- 61 -
6.1 Discussion.....	- 61 -
6.2 Future Work	- 62 -
REFERENCES	- 64 -
APPENDIX Signal Conditioning Circuit Schematics	- 67 -

LIST OF TABLES

Table 4-1 Measured Noise standard deviation (in μv)	- 49 -
---	--------

LIST OF FIGURES

Figure 2-1 Schematic representation of the generation of	- 5 -
Figure 2-2 Standard EMG recording system	- 6 -
Figure 2-3 Needle electrode [Neuman]	- 7 -
Figure 2-4 Wire electrode [Neuman]	- 8 -
Figure 2-5 MUs located close to the skin surface (1) produce a spatially steep.....	- 9 -
Figure 2-6 A schematic of the differential amplifier configuration [DeLuca02]	- 10 -
Figure 2-7 LDD filter of pin electrodes placed on the skin [Reucher87]	- 11 -
Figure 2-8 Four different EMG leads recording [Rau97]	- 12 -
Figure 2-9 Signal conditioner diagram	- 13 -
Figure 2-10 Differential amplifier with input sources [Hambley]	- 14 -
Figure 2-11 Measurement of differential gain	- 15 -
Figure 2-12 Measurement of common-mode gain.....	- 15 -
Figure 3-1 System schematic configuration [Clancy01]	- 17 -
Figure 3-2 The flow chart of equalization filter design	- 19 -
Figure 3-3 calibration data simulation model	- 21 -
Figure 3-4 simulation model of CMRR measurement.....	- 22 -
Figure 3-5 CMRR measurement configuration	- 25 -
Figure 3-6 Equalized channel outputs (absent noise)	- 27 -
Figure 3-7 Equalized channel outputs (1% noise)	- 28 -
Figure 3-8 Equalized channel outputs (3% noise)	- 29 -
Figure 3-9 CMRR vs noise level	- 30 -

Figure 3-10 Mixer system configuration	- 33 -
Figure 3-11 Equalization filter design model using mixing technique.....	- 35 -
Figure 3-12 CMRR measurement model.....	- 36 -
Figure 3-13 PSD plots for different CMRR (a) low CMRR, 40 dB, (b) high CMRR, 60 dB.....	- 37 -
Figure 3-14 CMRR measurement model.....	- 38 -
Figure 3-15 The mean and standard deviation of the error between the estimate and ideal-	40 -
Figure 3-16 The mean and standard deviation of the error of the estimate	- 40 -
Figure 3-17 The noise generated by two different amplifiers: TL084 and AD620	- 42 -
Figure 3-18 CMRR measurement configuration	- 43 -
Figure 3-19 Estimated CMRR and true CMRR.....	- 44 -
Figure 3-20 CMRR using linear shift technique.....	- 46 -
Figure 3-21 CMRR using windowing technique.....	- 47 -
Figure 4-1 Recording processing model.....	- 50 -
Figure 4-2 Calibration data.....	- 51 -
Figure 4-3 Calibration data after carving out the buffer	- 52 -
Figure 4-4 Configuration for equalization filter design.....	- 52 -
Figure 4-5 Magnitude response of the equalization filter.....	- 55 -
Figure 5-1 The schematic of one side of the array PCB board.....	- 57 -
Figure 5-2 The electrode array.....	- 57 -
Figure 5-3 28 channels EMG signal review	- 59 -
Figure 5-4 Equalized EMG signal (Bipolar) Right side is the zoomed view	- 59 -

Figure 5-5 Equalized EMG signal (NDD) Lower is the zoomed view..... - 59 -

Figure 5-6 EMG signal (NDD) before equalized - 60 -

Figure 5-7 EMG signal (NDD) after equalized - 60 -

CHAPTER 1 INTRODUCTION

1.1 *Project Objectives*

In recent years, surface electrode arrays have been developed to monitor the activity of motor units (MUs) — the smallest controllable portion of a skeletal muscle. There is an increasing interest in detecting single MU activity. Since it is hard to separate the activity of a single MU from the simultaneously active adjacent ones, the method of spatial filtering is used [Reucher86]. A spatial filtering is the weighted sum of several electrode recordings (or detection sites). Typically, spatial filtering is preformed in hardware. The accuracy of the weighting is measured in terms of common mode rejection ratio (CMRR). Ideally, the CMRR is infinite, but because of nonlinear characteristics and because components can never be exactly matched, typical CMRRs range from 60 to 120 dB at the fundamental power line frequency [Webster83].

With a hardware implementation, each different combination of detection sites requires a distinct hardware channel to apply precise weights. In such systems, the number of possibly useful derived signals can be too large for practical precision implementation in hardware. Since it is impossible to match the hardware characteristics of the distinct analog hardware channels, the number of electrode montages is limited for research. The objective of this project is to achieve high CMRR and flexible electrode combination via the use of software channel equalization. Similar equalization filters have been used in applications such as communication systems and radar.

As will be presented later, a bench-top prototype electrode array system with 5 channels and a printed circuit board prototype electrode array system with 28 channels

have been developed. Each channel in each array is designed with an identical analog signal conditioning circuit. Because of the component tolerances, the electrical characteristics for each hardware channel are necessarily different. These characteristics have been carefully measured to design the equalization filters. A distinct software equalization filter is cascaded with each hardware channel to correct for the channel difference. The software equalization filter is designed in the frequency domain. As will be shown in chapter 3, the issue with a conventional equalization technique is that it is very sensitive to noise. In this report, a new equalization design technique, termed our “mixing technique,” has been evaluated to achieve high CMRR.

1.2 Thesis Outline

The rest of thesis is organized as follows:

Chapter 2 provides some background information about the electromyogram (EMG) and its detection. This chapter focuses on the standard EMG detection system. Additionally, this chapter gives some details regarding existing high resolution spatial filters, the operating principle of spatial filters and their limitations in achieving high CMRR in hardware.

Chapter 3 gives the system model of the software channel equalization procedure. Section 3.1 explains the simple conventional technique to implement the equalization filter and provides simulation results to explain why it is necessary to find an improved technique. Section 3.2 gives the details of the new equalization filter implementation technique – the mixing technique used in the thesis – including the mixing algorithm, the low pass filter used in the system and the model for measuring CMRR.

Chapter 4 describes laboratory evaluation of the mixing technique using a five-channel prototype array system. Signal test sources are generated from a signal generator, passed through the analog signal conditioning circuits, and recorded using an A/D converter.

Chapter 5 introduces the 28-channel electrode array hardware system that is used to record the surface EMG signal from human subjects, including its hardware testing. Moreover, the chapter provides pilot experiment results of performing equalization on this array via the mixing technique.

Chapter 6 concludes the thesis with a discussion and summary. Some other possible methods to implement the equalization filters are described.

CHAPTER 2 BACKGROUND

This chapter provides fundamental information about EMG signals and the standard EMG detection systems. Additionally, different combinations of spatial filtering are introduced as well as the concept of CMRR measurement

2.1 EMG Introduction

In a skeletal muscle, a motor unit (MU) is the smallest functional unit, consisting of a single motor nerve and several muscle fibers. Under normal conditions, an action potential propagating down a motor neuron activates all the branches of the motor neuron [DeLuca79]; this action results in activating all the muscle fibers in that MU. When the postsynaptic membrane of a muscle fiber is depolarized, the depolarization propagates in both directions along the fiber; an electromagnetic wave is generated in the vicinity of the muscle fibers by the membrane propagation [DeLuca79]. An electrode located in this field can be used to detect the potential. This signal is called the electromyogram (EMG). Figure 2-1 models how the motor unit action potential (MUAP) is generated and recorded by electrode apparatus. The recorded EMG represents the superposition of MUs generated by each of the myofibrils. For standard surface recording of the EMG signal, its amplitude can range from 0 to 10 mV (peak to peak) or 0 to 1.5 mV RMS and most of the energy of the signal is limited from DC to 500 Hz with the dominant energy in the range of 15-150 Hz [DeLuca02].

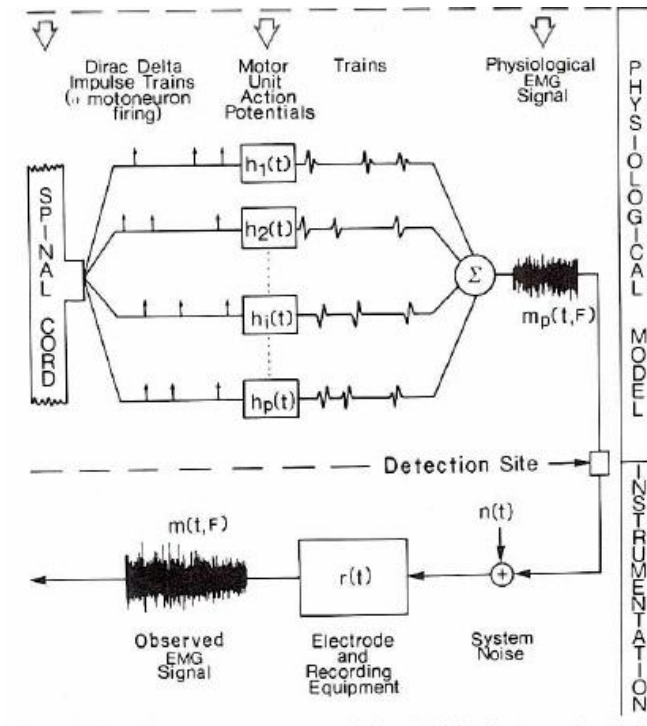


Figure 2-1 Schematic representation of the generation of the motor unit action potential [DeLuca79]

To detect single MU activity, high spatial resolution is required, because single MU activity has to be separated from the simultaneous activity of adjacent MUs [Disselhort98]. There are different approaches to detect the single MU activity. The most common approach is using a needle or a wire electrode. With this technique, the electrodes can be inserted into the muscle close to the desired location. Because of the short distance between the MUs and the small size of the electrode, a needle/wire electrode has high spatial resolution and single MU activity can be detected [Stalberg80]. But the insertion causes discomfort and creates the risk of infection [Disselhort98]. Additionally, the conventional needle/wire EMG techniques gain no information about the excitation spread across a muscle and long time monitoring is not possible

[Disselhort98]. Moreover, the inserted needle/wire disturbs the electrical field which is generated by the MU.

For these reasons, the detection of the single MU activity at the skin surface becomes increasingly attractive. The conductive electrode which is used to detect the surface EMG is much larger than the needle electrode and can be placed a long distance away from the desired sites, but this causes the conventional surface EMG signal to be a superposition of a large number of MUs [Rau97]. So, the conventional surface EMG has a limited spatial selectivity.

2.2 Standard EMG Array Detection System

For technical reasons, the recording electrode for the typically EMG is bipolar and the signal is amplified differentially [DeLuca79]. A standard EMG recording system is shown as Figure 2-2.

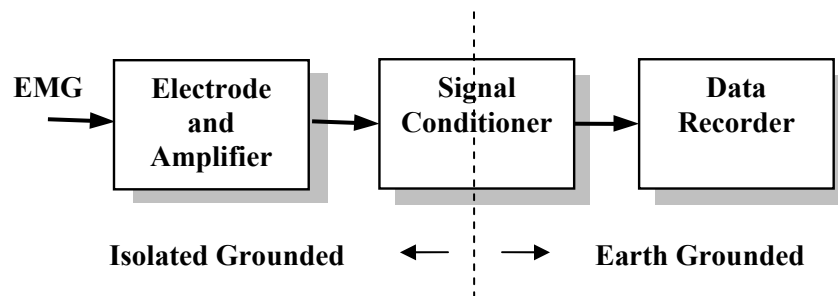


Figure 2-2 Standard EMG recording system

Electrode and Amplifier

In general, conductive electrodes are used to detect EMG. They can be either a surface electrode, which is located on the skin surface overlying the muscle, or an indwelling electrode, which is inserted into the muscle. There are two kinds of indwelling electrodes: needle and wire.

Needle electrodes are used to penetrate the skin and tissue to reach the desired sites. As stated above, the advantage of using needle electrodes is that, due to the short distance between the MU and the recording sites, the spatial resolution is high enough to detect the single MU activity [Disselhort98]. It also can be repositioned within the muscle. The disadvantage of this technique is the discomfort and risk of infection because of the insertion. Figure 2-3 shows typical needle electrodes.

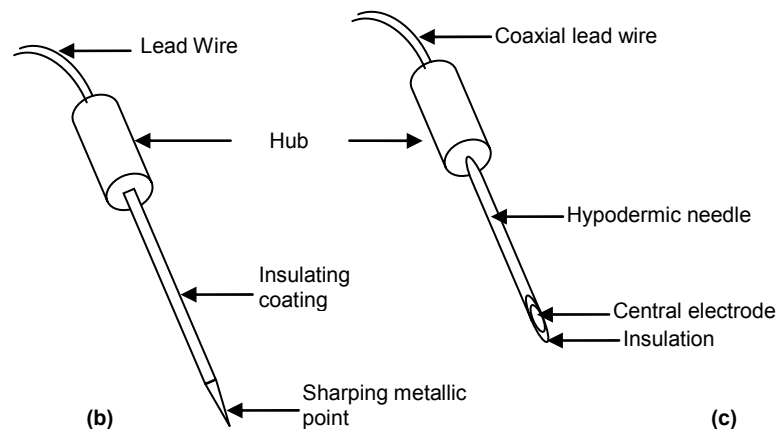


Figure 2-3 Needle electrode [Neuman]

Wire electrodes are smaller than needle electrodes. A hypodermic needle is used to hold the wire electrode and insert it through the skin into the muscle at the desired site. The advantage of using a wire electrode is that it can access deep musculature and detect the single MU activity with little cross-talk (the absence of cross-talk means that the signal sources close to the electrode will dominate the recorded EMG signal [Scott])

concern. The disadvantage is that it is extremely sensitive and it may require medical personnel for insertion. Additionally, it is almost impossible to reposition wire electrodes back in their original site once they are moved or removed. Due to their small size, the detection area may not represent the entire muscle. Figure 2-4 shows an example of this other type of electrode: the wire electrode.

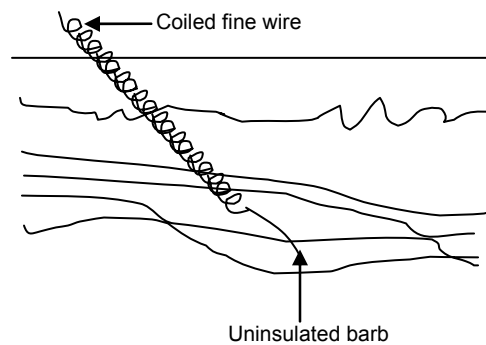


Figure 2-4 Wire electrode [Neuman]

Because of the limitations of the needle technique, the surface electrode becomes more and more attractive. A surface electrode is considerably much larger than an indwelling electrode, so it has a limited spatial resolution and detects the superimposed activity of a large number of MUs. The advantage of using a surface electrode is that it can be easily applied without any pain and doesn't require medical supervision.

In recent years, due to the use of spatial filtering, the separation of single MU activity from simultaneously active adjacent MUs has become possible. The new technique uses surface electrode arrays in combination with different spatial filter processing to improve the spatial resolution. In this way, detecting single MU activity can be achieved in a noninvasive manner [Reucher87].

The principle of spatial filtering is based on the fact that the potential distribution on the skin surface has a spatially steep gradient [Rau97]. Any spatial filtering must have

an inverting and a noninverting part, and the sum of the channel weights must equal zero to eliminate the powerline interference. Figure 2-5 shows the potential contributed by MUs located close to the skin surface. It shows a bipolar lead with small sized electrodes separated by a few millimeters and arranged parallel to the muscle fibers. It forms the lowest order spatial filter — the bipolar configuration — which differentiates the potential distribution in the direction of the electrode configuration. The operation of the bipolar filter is very simple. It differentiates the potential distribution generated on the skin surface, and then amplifies the difference. Thus, it is also called a pre-amplifier. A schematic of this configuration is shown as Figure 2-6. The EMG signal is represented as “m” and the common interference signal is represented as “n”.

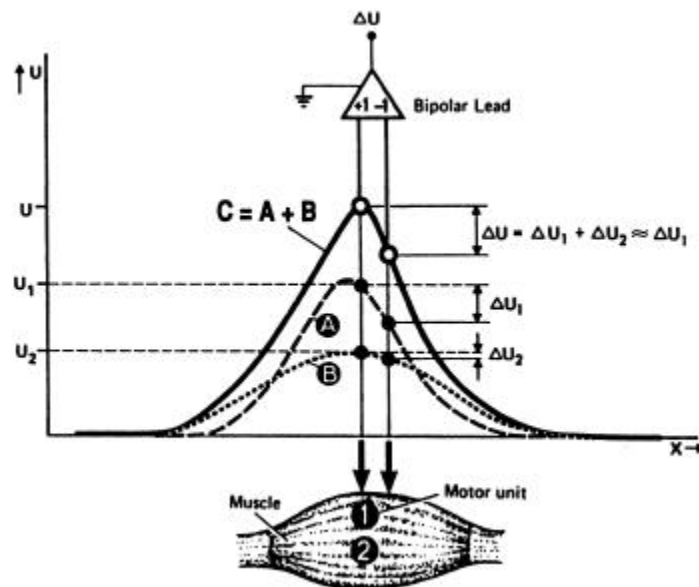


Figure 2-5 MUs located close to the skin surface (1) produce a spatially steep potential gradient (A) in the recording area; (2) a flat potential course. Using a bipolar lead with a small interelectrode distance the flat potential course contributes only with a small part (ΔU_2) to the measured total value (ΔU) [Rau97]

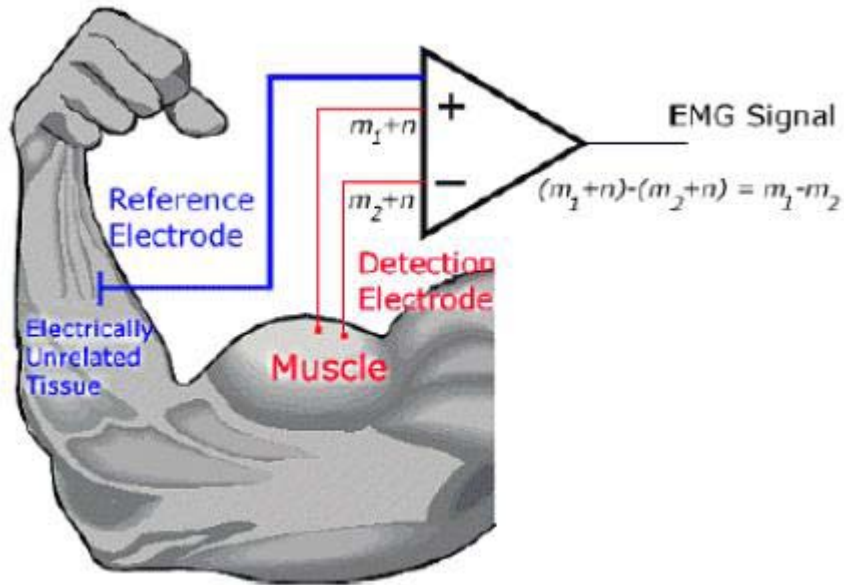


Figure 2-6 A schematic of the differential amplifier configuration [DeLuca02]

Due to the spatial filtering, the bipolar lead can detect the single MU activity at a very low contraction level [Rau97]. It is not sufficient to detect the single MU activity at high level contractions. Therefore, the spatial filtering approach has been extended one or more dimensions, such as the longitudinal double differentiating filter (LDD-filter) and the normal double differentiating filter (NDD-filter).

The LDD filter performs spatial double differentiation of the potential distribution [Reucher87] [Reucher87b]. It is formed by three successive electrodes, which are arranged equidistant along a line with weighting coefficients (+1, -2, +1). Figure 2-7 shows the performance of the LDD filter. In this experiment, a longitudinal array with equidistant electrodes (distance 2.5mm) is placed on the skin. This figure demonstrates the advantage of using the LDD filter instead of bipolar or monopolar montages. The signals show the differences in the selectivity of different sizes of pickup area. In the upper two traces, the filter output signal shows a sharp positive peak when the negative maximum of the potential wave accompanying a MU excitation is at the center electrode

at the LDD filter [Reucher87]. In spite of the high contraction level, the impulses of four different MU's (labeled A, B, C and D in the figure) can be distinguished by their amplitude and their direction of propagation [Reucher87]. In the lower two traces, single MU's cannot be separated because many MU's are simultaneously discharging. This figure shows the advantages of recording with selective spatial filters.

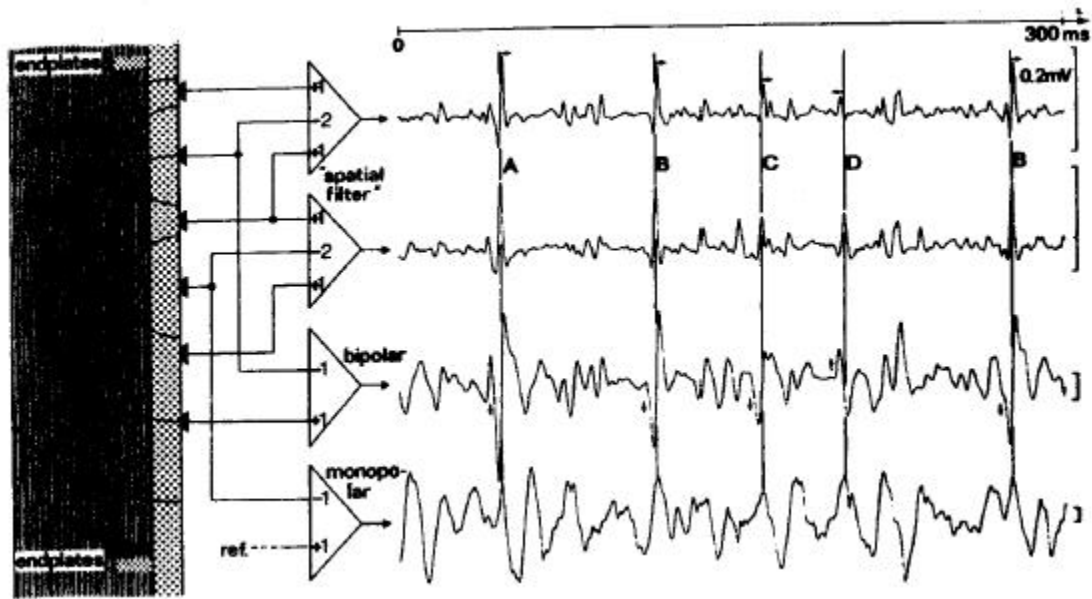


Figure 2-7 LDD filter of pin electrodes placed on the skin [Reucher87]

The NDD filter (a.k.a. a Laplace filter) is well suited for the detection of edges perpendicular to the direction of the differentiation [Disselhorst97]. It is formed by a weighted summation of five crosswise-arranged electrodes. The weighting factors of each electrode are represented by the filter mask [Disselhorst97]

$$M_{NDD} = \begin{pmatrix} 0 & 1 & 0 \\ 1 & -4 & 1 \\ 0 & 1 & 0 \end{pmatrix}.$$

The rows and the columns of the filter mask are identical to the rows and columns of the electrode array.

Figure 2-8 compares the performance for four different EMG spatial filters using data recorded from the m. abductor pollicis brevis muscle at maximum voluntary contraction. It shows that the bipolar electrode does not sufficiently distinguish individual MU activity at high contraction level but the NDD can separate the single MU activity. As the spatial filtering extended to three or more electrodes, the spatial selectivity improved. The NDD filter improves the spatial selectivity in all directions and can detect single MU activity even at maximum voluntary contraction.

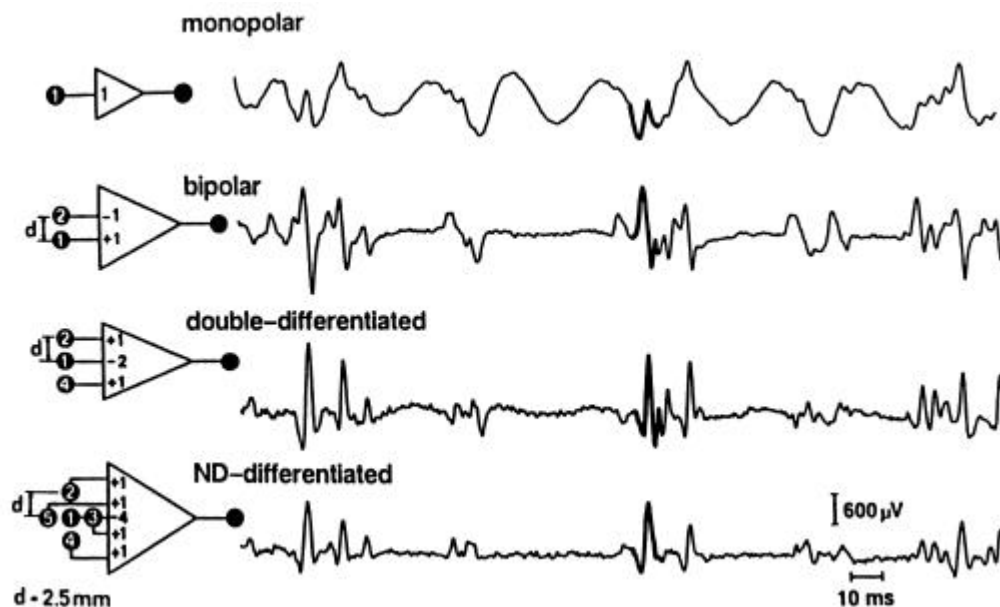


Figure 2-8 Four different EMG leads recording [Rau97]

Signal Conditioner

Figure 2-9 shows a system-level diagram of a signal conditioner. In general, the signal conditioner consists of a high pass filter, which attenuates motion artifact and any offset potentials; selectable gain, which magnifies the signal up to the range of the data recording/monitoring instrumentation; electrical isolation, which prevents injurious

current from entering the patient; and a low pass filter, which prevents anti-aliasing and attenuates noise out of the physiologic frequency range.

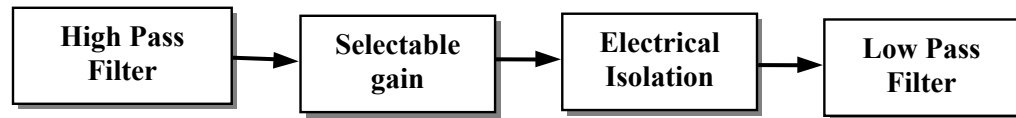


Figure 2-9 Signal conditioner diagram

2.3 Common Mode Rejection Ratio (CMRR)

2.3.1 Definition

CMRR is defined as the ratio of the magnitude of the differential gain to the magnitude of the common mode gain of two channels. Often, CMRR is expressed in dB as

$$CMRR = 20 \log_{10} \left(\frac{|G_d|}{|G_c|} \right) \quad \text{Equation 2-1}$$

where G_d is the magnitude of the differential signal and G_c is the magnitude of the common signal. Ideally, the CMRR is infinite, but for the existing equipment, because of nonlinear characteristics and because components can never be exactly matched, typical CMRRs range from 60 to 120 dB at the fundamental power line frequency [Webster83].

2.3.2 Measurement of CMRR

Differential Amplifier [Hambley]

For two input signals, an ideal differential amplifier is shown in Figure 2-10.

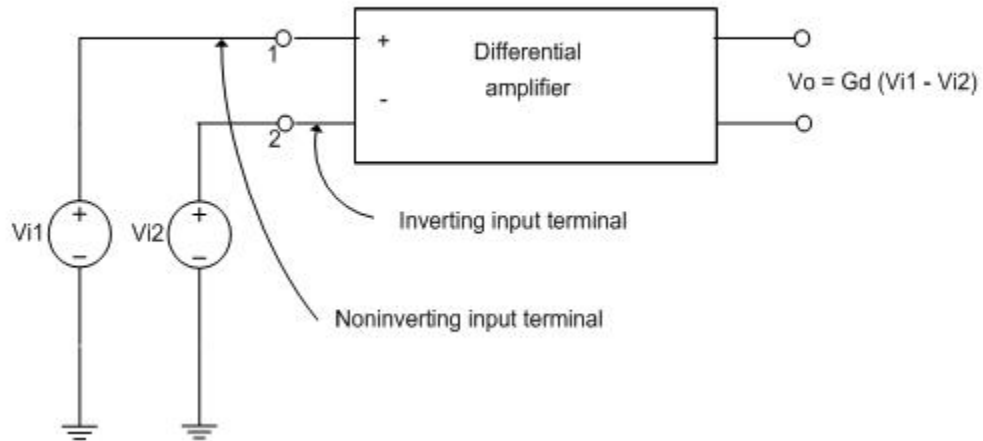


Figure 2-10 Differential amplifier with input sources [Hambley]

The difference between the input voltages is amplified by gain G_d , giving the output voltage (V_o) as:

$$V_o = G_d (V_{i1} - V_{i2}) = G_d V_{i1} - G_d V_{i2} \quad \text{Equation 2-2}$$

The difference between the input voltages V_{i1} and V_{i2} is known as the differential signal v_{id} .

$$V_{id} = V_{i1} - V_{i2} \quad \text{Equation 2-3}$$

We refer to the gain G_d as the differential gain. So, the output of the ideal differential amplifier can be written as

$$V_o = G_d V_{id} \quad \text{Equation 2-4}$$

The input sources v_{i1} and v_{i2} can be replaced by the equivalent sources v_{icm} and v_{id} , where v_{icm} is the common mode signal and is given by

$$V_{icm} = \frac{1}{2}(V_{i1} + V_{i2}) \quad \text{Equation 2-5}$$

Measurement of differential gain

A practical measurement of differential gain is shown in Figure 2-11

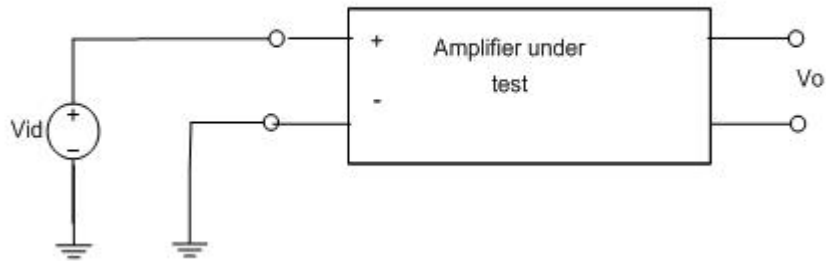


Figure 2-11 Measurement of differential gain

According to Equation 2-4, the differential gain can be calculated from

$$G_d = \frac{V_o}{V_{id}} \quad \text{Equation 2-6}$$

Measurement of common-mode gain

The practical measurement of common-mode gain is shown as Figure 2-12

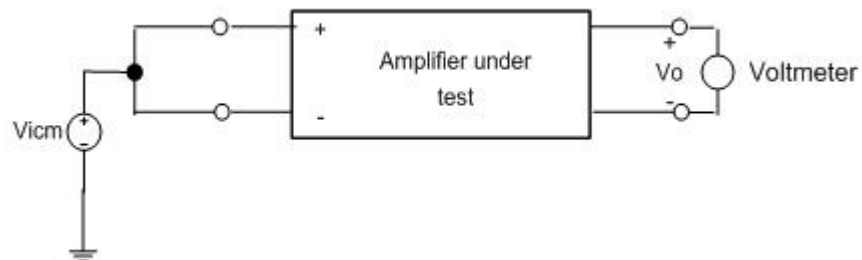


Figure 2-12 Measurement of common-mode gain

The common-mode gain can be calculated from

$$G_c = \frac{V_o}{V_{icm}}$$

Equation 2-7

where v_{icm} can be calculated from Equation 2-5.

The higher the CMRR, the better the performance of the subtraction process within the amplifier. For bipolar electrodes, CMRR is the ratio of the common-mode interference voltage at the input of a circuit, to the corresponding interference voltage at the output. As shown in Figure 2-6, the signals are detected at two sites, subtracted by the differential amplifier and gain amplified. With this operation, any signal that is “common” to both sites will be removed and any signal that is different will be amplified. Thus, relatively distant power line interference signals (which appear as common signals at each electrode) will be removed and relatively local EMG signals will be amplified [DeLuca02]. In practice, it is very difficult to remove the common signal perfectly. In general, the subtraction is performed in hardware. Currently, we can achieve CMRRs as high as 120 dB with hardware. But there are limitations with hardware implementations, such as high expense, the requirement to build a separate circuit for each spatial channel desired, and that power line interference does not present an exactly common signal to each electrode site.

CHAPTER 3 Simulation of Equalization Filters

The purpose of this project is to implement equalization filters in software to achieve high CMRR. Figure 3-1 shows the general system configuration. For the hardware system, a 5-channel bench-top prototype and a 4x7 equal-spaced rectangular array prototype have both been developed. For both, each channel is designed with an identical analog circuit design. All of the resistors have 1% tolerance and the capacitors have 5% tolerance. A distinct software equalization filter is cascaded with each signal conditioner circuit.

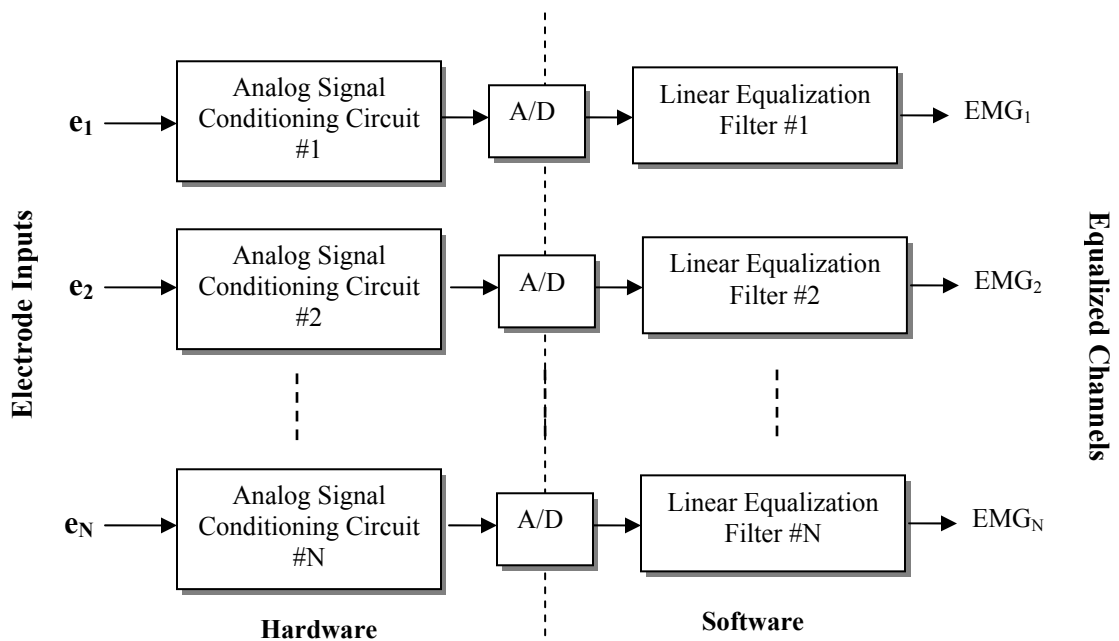


Figure 3-1 System schematic configuration [Clancy01]

In general, the equalization filter is determined by measuring the frequency-dependent gain and phase of each analog signal conditioning channel. The desired (“ideal”) frequency response divided by the measured frequency response gives the frequency response of the equalization filter. After the frequency response of the

equalization filter H_e is achieved, a FIR filter with order $2L + 1$ is designed (to be used to implement the filter in the time domain).

Note that the impulse response of the equalization filter, using the transfer function approach, must be real-valued. To prove this assertion, begin by assuming that the output of the reference channel is $x(t)$ and the output of the equalized channel is $y(t)$. By using the transfer function approach, the frequency response of the equalization filter $H(w)$ can be written as in Equation 3-1.

$$H(w) = \frac{Y(w)}{X(w)} \quad \text{Equation 3-1}$$

Notice that both $y(t)$ and $x(t)$ are real signals. For real signal $x(t)$, its transform must be of the form

$$X(w) = X_R(w) + jX_I(w) \quad \text{Equation 3-2}$$

where $X_R(w) = \sum_{n=-\infty}^{\infty} x(n)\cos wn$ and $X_I(w) = \sum_{n=-\infty}^{\infty} x(n)\sin wn$ [Proakis96, P287]. It follows that

$$\begin{aligned} X_R(-w) &= X_R(w) \\ X_I(-w) &= -X_I(w) \end{aligned}$$

Similarly with the reference channel,

$$\begin{aligned} Y_R(-w) &= Y_R(w) \\ Y_I(-w) &= -Y_I(w) \end{aligned}$$

The transform

$$\begin{aligned} H(w) &= H_R(w) + jH_I(w) = \frac{Y(w)}{X(w)} \\ &= \frac{Y_R(w) + jY_I(w)}{X_R(w) + jX_I(w)} \\ &= \frac{Y_R(w)X_R(w) + Y_I(w)X_I(w)}{X_R^2(w) + X_I^2(w)} + j \frac{Y_R(w)X_I(w) - Y_I(w)X_R(w)}{X_R^2(w) + X_I^2(w)} \end{aligned}$$

So, we get that

$$H_R(w) = \frac{Y_R(w)X_R(w) + Y_I(w)X_I(w)}{X_R^2(w) + X_I^2(w)}$$

$$H_I(w) = \frac{Y_R(w)X_I(w) - Y_I(w)X_R(w)}{X_R^2(w) + X_I^2(w)}$$

$$H_R(-w) = \frac{Y_R(-w)X_R(-w) + Y_I(-w)X_I(-w)}{X_R^2(-w) + X_I^2(-w)}$$

$$= \frac{Y_R(w)X_R(w) + [-Y_I(w)]X_I(w)}{X_R^2(w) + X_I^2(w)}, \text{ and}$$

$$= \frac{Y_R(w)X_R(w) + Y_I(w)X_I(w)}{X_R^2(w) + X_I^2(w)}$$

$$= H_R(w)$$

$$H_I(-w) = \frac{Y_R(-w)X_I(-w) - Y_I(-w)X_R(-w)}{X_R^2(-w) + X_I^2(-w)}$$

$$= \frac{-Y_R(w)X_I(w) + Y_I(w)X_R(w)}{X_R^2(w) + X_I^2(w)}$$

$$= -H_I(w)$$

Thus, we can say that the impulse response $h_e(n)$ of the equalization filter must be real.

In this report, two filter design methods will be introduced to form the FIR filter based on the frequency response. The first method is the windowing technique. Figure 3-2 shows the diagram of this method.



Figure 3-2 The flow chart of equalization filter design

In general, the coefficients of the $(2L+1)$ th order FIR filter can be obtained by truncating the sequence $h_e(n)$ at point $2L+1$. Truncation of $h_e(n)$ to a length $2L+1$ is equivalent to using a “rectangular window” [Proakis96]. Other window functions can also be used in this stage such as a “hamming window” or “hanning window”. Thus, the time-domain filter, $b(n)$ can be formed as

$$b_n \subset h_e(n) \quad n = 1, 2, \dots, 2L + 1$$

Equation 3-3

The second method consists of implementing a linear shift (advance) of the input sequence by half the FIR filter order before the frequency response of the equalization filter is calculated. The reason for this shift is that the signals propagating through a physical hardware channel can either lag or *lead* the phase of a signal propagating through an ideal channel. Without this linear shift, significant power can result at the end of the impulse response (due to the frequency response representing a non-causal signal propagation), but will be discarded with the simple windowing technique. Later, we will show the results using these two equalization filter designs.

3.1 Conventional technique

To determine the frequency response of the equalization filter using our “conventional” technique, the desired (“ideal”) frequency response is divided by the measured frequency response. In this section, we will illustrate the simulation results for this conventional technique and show that this technique is not sufficient to achieve high CMRR. Also, we will present the new technique – a mixing technique – comparing these two techniques. First, we will introduce the conventional technique.

3.1.1 Equalization Filter Frequency Response

To simplify the problem in simulation, we suppose there are three channels. All the simulations are performed in Matlab. The third channel is our reference channel (“ideal” channel), and the first two channels are equalized to the reference channel. These two channels simulate the bipolar electrode. Each channel has the same characteristics: a

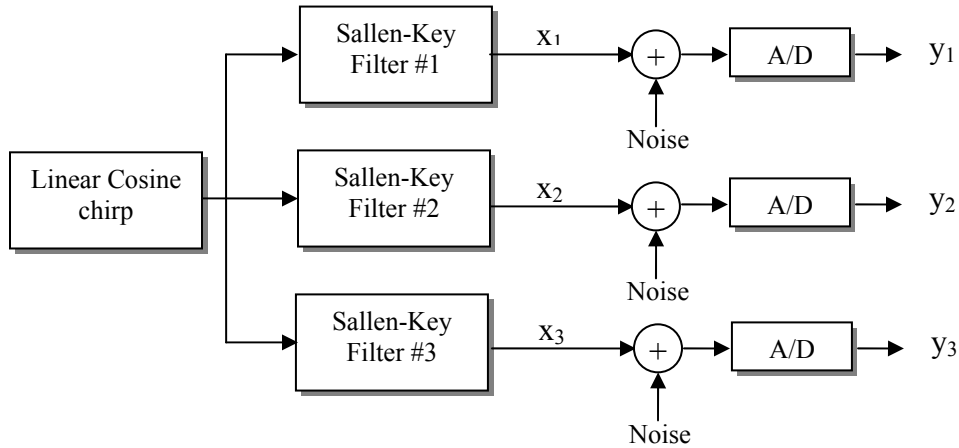


Figure 3-3 calibration data simulation model

fourth-order Sallen-Key high pass filter [Texas] with cut-off frequency at 15 Hz cascaded with a four-order Sallen-Key low pass filter with cut-off frequency at 1800 Hz. Both the low pass and high pass filters have unit gain. All of the components in the three channels have the same mean value with a 5 percent tolerance. To measure the frequency response of the equalization filter, the three channels are excited with a cosine chirp signal which ranges in frequency from 0 to 2K Hz. Figure 3-3 shows the simulation configuration. For each simulation, the cosine chirp is always $3\cos(2\pi * 100t^2)$ V and a sampling frequency of 4096 Hz is used. The A/D converter is modeled as an ideal signal sampler. The noise input is white Gaussian noise.

For this simulation, y_3 is our “ideal” signal. For the other two channels, the frequency response of the software equalization filter H_e can be calculated by Equation

3-4, where i is the channel number. In this project, the length of the data sequence is 409600.

$$H_e^{(i)} = \frac{\text{fft}(y_3)}{\text{fft}(y_i)} \quad \text{Equation 3-4}$$

3.1.2 CMRR Measurement

3.1.2.1 Equivalent CMRR Measurement

The CMRR measurement model in this report is shown in Figure 3-4

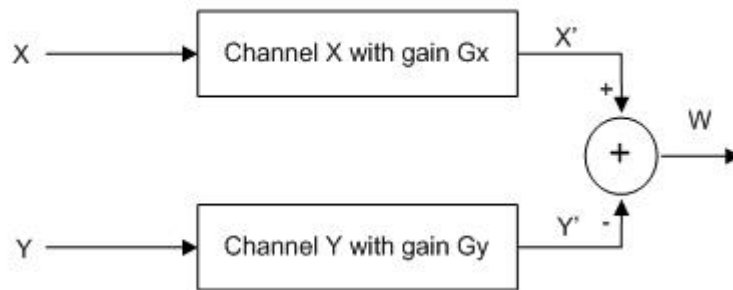


Figure 3-4 simulation model of CMRR measurement

Here we assume that,

- Every channel is a linear system at frequency w_0 .
- Signal X, Y, X' and Y' are voltage phasers.
- Both G_x and G_y are complex number gains.

Note that our CMRR measurements are made at a fixed frequency.

Measurement of common-mode gain in simulation

We apply V_c (voltage phaser, i.e., a sinusoid) to both channels X and Y . Thus the common mode gain is

$$|G_c| = \frac{|W|}{|V_c|} \quad \text{Equation 3-5}$$

The summation in Figure 3-4 takes the difference of its inputs. Therefore

$$W = X' - Y' = V_c \cdot G_x - V_c \cdot G_y = V_c(G_x - G_y) \quad \text{Equation 3-6}$$

Applying Equation 3-6 to Equation 3-5, we can get the common-mode gain

$$|G_c| = \frac{|V_c(G_x - G_y)|}{|V_c|} = |G_x - G_y| \quad \text{Equation 3-7}$$

Measurement of differential gain in simulation

To measure the differential gain, we apply $\frac{V_d}{2}$ to input X and $-\frac{V_d}{2}$ to input Y . Then the differential gain can be written as

$$|G_d| = \frac{|W|}{|V_d|} \quad \text{Equation 3-8}$$

where W can be written as

$$W = \frac{V_d}{2} \cdot G_x + \frac{V_d}{2} \cdot G_y = \frac{V_d}{2}(G_x + G_y) \quad \text{Equation 3-9}$$

Substituting Equation 3-9 into Equation 3-8, we can get the common-mode gain

$$|G_d| = \frac{\left| \frac{V_d}{2}(G_x + G_y) \right|}{|V_d|} = \frac{1}{2}|G_x + G_y| \quad \text{Equation 3-10}$$

Applying Equation 3-10 and Equation 3-7 to Equation 2-1, we can get

$$CMRR = 20 \log_{10} \left(\frac{|G_x + G_y|}{2 \cdot |G_x - G_y|} \right) \quad \text{Equation 3-11}$$

Because we use a single-ended amplifier in our simulation, if we apply a common signal V_c in,

$$\begin{aligned} X' &= V_c \cdot G_x \Rightarrow G_x = X' / V_c \\ Y' &= V_c \cdot G_y \Rightarrow G_y = Y' / V_c \end{aligned} \quad \text{Equation 3-12}$$

Substituting Equation 3-12 into Equation 3-11, we get

$$CMRR = 20 \log_{10} \left(\frac{|X'+Y'|}{2 \cdot |X'-Y'|} \right) \quad \text{Equation 3-13}$$

3.1.2.2 CMRR Measurement Model

After obtaining the coefficients of the equalization filter in the time domain for each channel, we evaluated their performance by measuring the CMRR. Figure 3-5 shows the CMRR measurement configuration. Since the dominant interference from the power lines is at 60 Hz (or 50 Hz in some regions outside of North America) [DeLuca02], the CMRR at 60 Hz is measured. In this simulation, we excite the first and second channel with a 60 Hz sine waveform, which then passes through the Sallen-Key filter and the equalization filter. The signals y_{e1} and y_{e2} are the equalized channel outputs. With ideal equalization (infinite CMRR), the signals would be zero-valued at all times (at least in the absence of any noise). Using Equation 3-13, we can measure the CMRR.

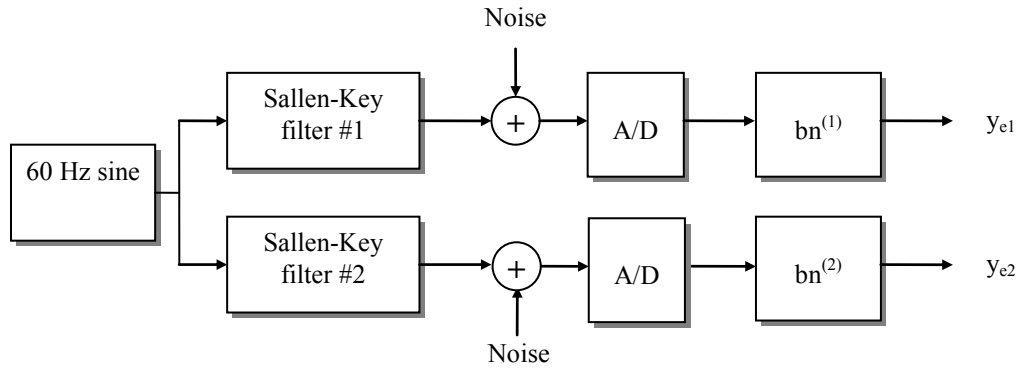


Figure 3-5 CMRR measurement configuration

By using Equation 3-13, the CMRR between the two outputs y_{e1} and y_{e2} can be written as

$$CMRR = 20 \log_{10} \left(\frac{|A_d|}{2 \cdot |A_c|} \right) \quad \text{Equation 3-14}$$

where A_d is the magnitude of the sum of the two output signals y_{e1} and y_{e2} at 60Hz and A_c is the magnitude of the difference between the two output signals at 60Hz. Define $s(t) = y_{e1}(t) + y_{e2}(t)$ and $c(t) = y_{e1}(t) - y_{e2}(t)$. In practice, for the sum of the two signals $s(t)$, it is easy to measure its magnitude at 60 Hz. But, if the two signals are matched precisely, it is hard to measure the magnitude of the difference of the signals $c(t)$, particularly in the presence of noise.

One way to measure the amplitude of the signal $y_{e1}(t) - y_{e2}(t)$ is via direct measure of its power at 60 Hz from the power spectral density of the differential signal $c(t)$. The drawback of this technique is that in order to accurately measure the PSD at 60 Hz, the noise level must be significantly lower than the signal level at this frequency. For CMRRs above 40–50 dB, which means the difference between the two channels are smaller, the noise is larger than the 60 Hz signal when we subtract the two channels.

However, the power spectrum technique was sufficient for CMRR measurement for conventional equalization.

3.1.3 Simulation Results For The Conventional Technique

In this section, we present the simulation results for the conventional equalization technique. We will show that the main problem is its sensitivity to noise. In this simulation, we will vary the noise level to see how the noise affects the performance of the system.

Absent noise

In this simulation, we set the noise level to zero. After the frequency response of the filter is measured, a FIR filter is designed using the simple windowing technique (i.e., absent the linear shift operation). Figure 3-6 shows the difference between the two equalized channel outputs. From the previous discussion, the major issue that affects CMRR is the background noise. Since the noise level is zero, the CMRR should be infinite (ideally). There is no quantization noise in this simulation since an all pass filter is used instead of a quantizer.

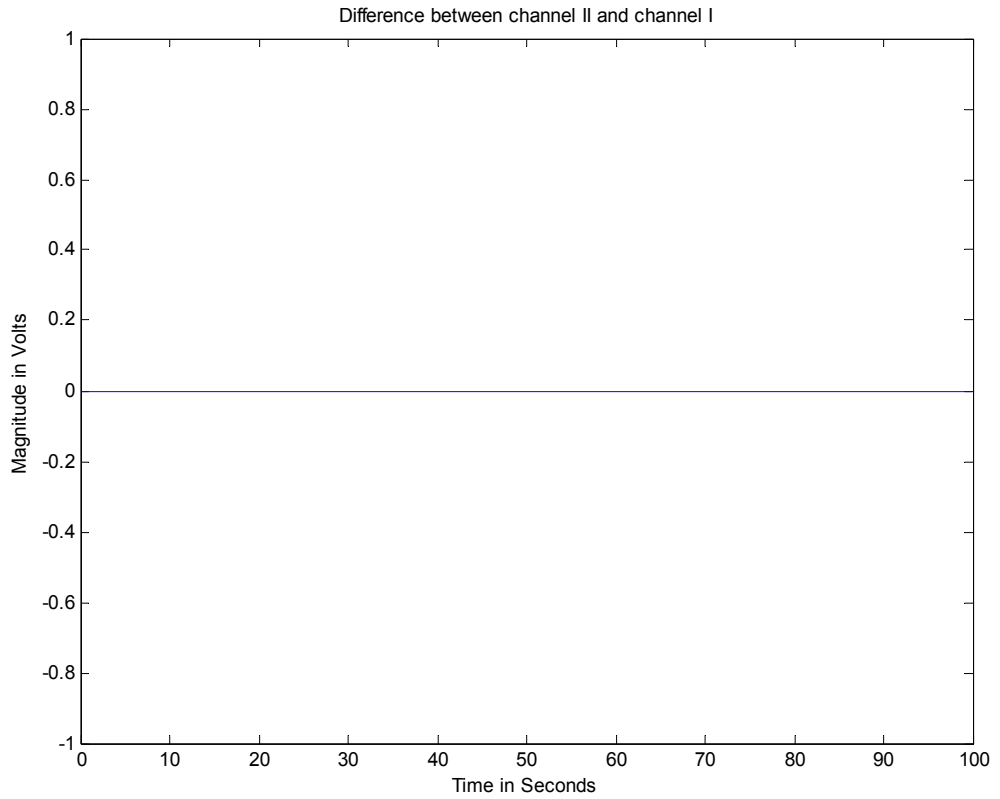


Figure 3-6 Equalized channel outputs (absent noise)

1 percent noise

Next, we set the standard deviation of the background noise level to 1 percent of the input signal amplitude. The resulting CMRR is around 40 dB. Plots showing this simulation, following the format described above, are shown in Figure 3-7.

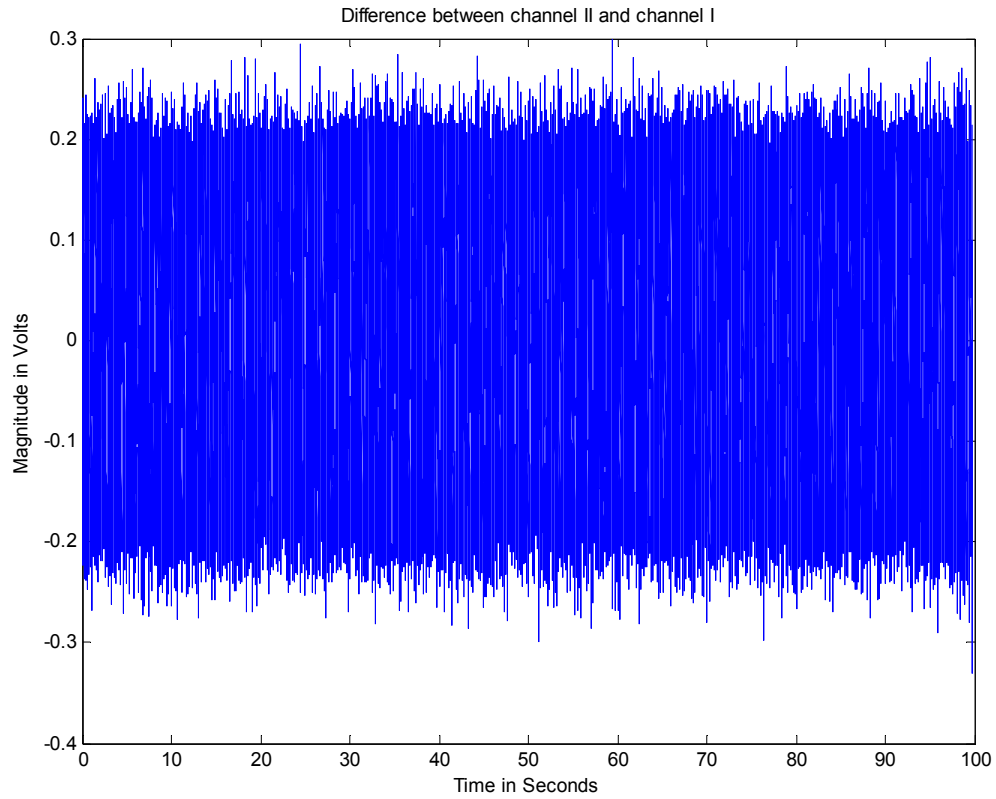


Figure 3-7 Equalized channel outputs (1% noise)

3 percent

Lastly, the noise standard deviation was increased to 3 percent of the input signal amplitude. The resulting CMRR is around 25 dB. Plots showing this simulation, following the format described above, are shown in Figure 3-8.

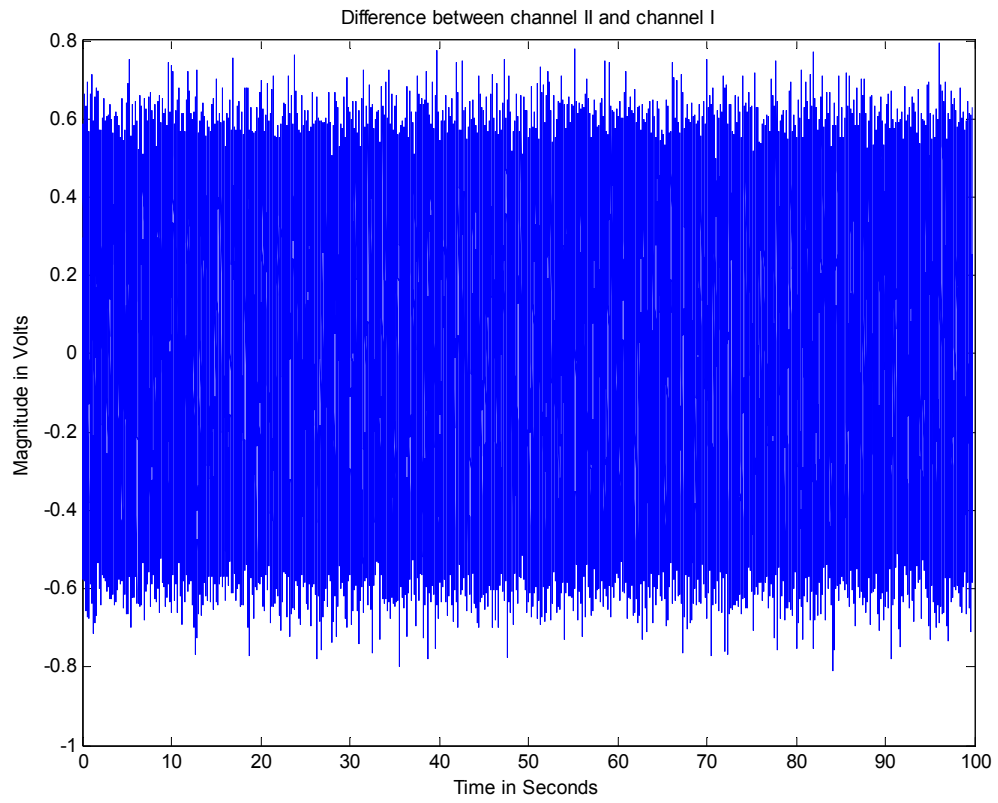


Figure 3-8 Equalized channel outputs (3% noise)

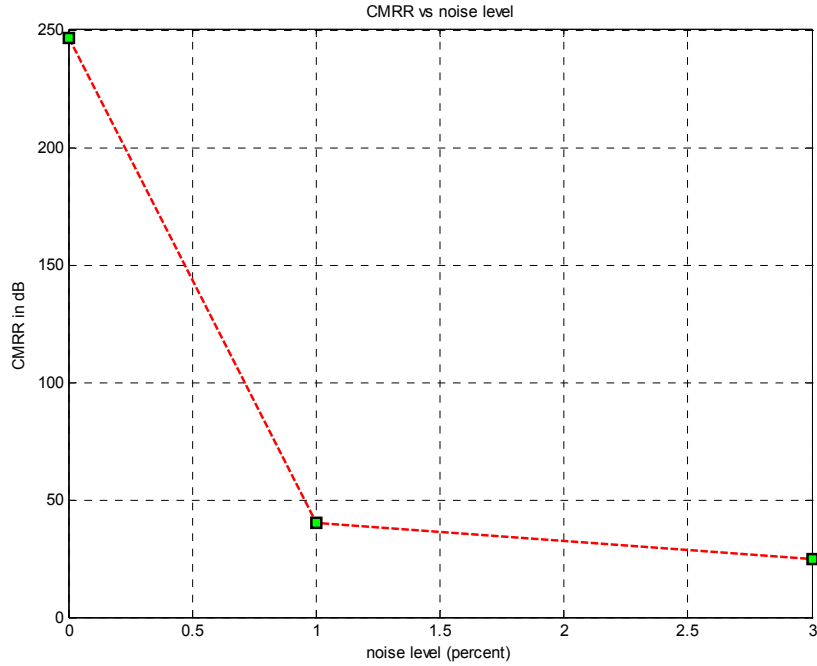


Figure 3-9 CMRR vs noise level

Figure 3-9 shows CMRR becomes lower and lower when the noise level is increasing. From these results, we can see that absent noise, an excellent CMRR is achieved. However, even a small amount of noise severely degrades the CMRR performance. Since state-of-the art EMG hardware has noise at or above the levels tested here, this technique is too sensitive to the noise level. It is not a practical method for achieving high CMRR, thus an alternative equalization filter design technique was explored.

3.2 *Mixing Technique*

Based on the discussion in the previous section, the conventional technique that calibrates the equalization filter directly from the measured data is very sensitive to noise,

which results in low CMRR. It is necessary to find a new technique that is less sensitive to the noise and can be easily implemented in software. As we have found, the major impediment to achieving high CMRR is the broadband background noise which cannot be eliminated within the hardware. Certainly, the hardware should eliminate as much noise as possible. We focused on a signal processing method, based on a mixing technique common in communications engineering, to remove noise from the signals.

3.2.1 Mixing Algorithm

In using this technique, we assume that the input signal is a linear chirp with a fixed magnitude and sweeping rate. The premise of this technique is mixing the measured chirp waveform with another chirp waveform that has the same sweep rate and initial frequency. The resultant outputs will be the sum of two chirps – one with double the sweep rate which can be filtered out by a proper low pass filter, and one with a zero sweep rate (DC signal) which contains all the magnitude and phase information of the measured chirp waveform. In this section, we will introduce the mixing algorithm and how to choose the proper parameters for the mixer.

Chirp Presentation

A linear chirp can be written as

$$\text{linear chirp} = \text{Re} \left[A e^{j(w_0 t + w t^2 + \theta)} \right] \quad \text{Equation 3-15}$$

By using Euler's identity

$$\text{Re} \left[e^{j w t} \right] = \cos(w t) = \frac{e^{j w t} + e^{-j w t}}{2}$$

the linear chirp can be re-written as

$$\text{linear chirp} = \frac{A}{2} \left[e^{j(w_0 t + wt^2 + \theta_n)} - e^{-j(w_0 t + wt^2 + \theta_n)} \right] \quad \text{Equation 3-16}$$

where w_0 , w , θ are constants. The instantaneous angular frequency is

$$w_{inst} = \frac{d(w_0 t + wt^2 + \theta_n)}{dt} = w_0 + 2wt \quad \text{Equation 3-17}$$

Let $w_0 = 2\pi b$, $w = 2\pi a$, where a (Hz/s), and b (Hz) are scaling constants. Hence the linear chirp can also be written as

$$\text{linear chirp} = \frac{A}{2} \left[e^{j(2\pi a t^2 + 2\pi b t + \theta_n)} - e^{-j(2\pi a t^2 + 2\pi b t + \theta_n)} \right] \quad \text{Equation 3-18}$$

and has an instantaneous frequency of

$$f = 2at + b \quad \text{Equation 3-19}$$

For example, a ten-second linear chirp formed by selecting $a = 100$ and $b = 0$ would begin at 0 Hz and end at 2 K Hz.

More generally, if such a chirp is passed through a linear system, the output $s(t)$ is also a chirp, but can be modified in magnitude and phase at each frequency and embedded in an independent additive noise. Let the input $w(t)$ to the linear system be written as

$$w(t) = \frac{A_{in}}{2} \left[e^{j(2\pi a t^2 + 2\pi b t + \theta_n)} - e^{-j(2\pi a t^2 + 2\pi b t + \theta_n)} \right] \quad \text{Equation 3-20}$$

Since the frequency of the input chirp has a direct (and known) relation to time, the magnitude and phase distortion imposed by the linear system can be captured by the time variant magnitude $A(t)$ and phase $\theta(t)$ of the output, written as

$$s(t) = \frac{A(t)}{2} \left[e^{j(2\pi at^2 + 2\pi bt + \theta(t))} - e^{-j(2\pi at^2 + 2\pi bt + \theta(t))} \right] + n(t) \quad \text{Equation 3-21}$$

where $n(t)$ is the additive noise, $A(t) = \frac{A_{out}(t)}{A_{in}}$ is the magnitude distortion (a value of one for a given time indicates no magnitude distortion, a value greater than one indicates that the linear system amplifies the signal, and a value less than one indicates that the linear system attenuates the signal) and $\theta(t) = \theta_{out}(t) - \theta_{in}$ is the phase modulation (a value of zero radians for a given time indicates no phase distortion, a value greater than zero indicates an induced phase lag).

Mixing Algorithm

Based on the previous discussion, the mixer configuration is shown in Figure 3-10,

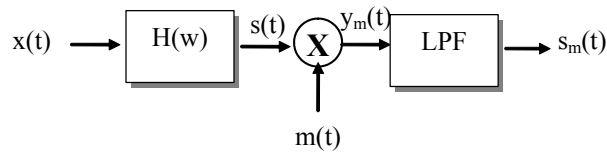


Figure 3-10 Mixer system configuration

where the input signal $x(t) = \frac{A_{in}}{2} \left[e^{j(2\pi at^2 + 2\pi bt + \theta_{in})} - e^{-j(2\pi at^2 + 2\pi bt + \theta_{in})} \right] + n_{in}(t)$, $H(w)$ is a linear system and the mixer $m(t) = -2e^{j(2\pi \alpha t^2 + 2\pi \beta t + \theta_m)}$ where α (Hz/s), and β (Hz) are scaling constants.

Using Equation 3-21, the output $s(t)$ of the linear system is written as

$$s(t) = \frac{A_{out}(t)}{2} \left[e^{j(2\pi at^2 + 2\pi bt + \theta)} - e^{-j(2\pi at^2 + 2\pi bt + \theta_{out}(t))} \right] + n_{out}(t)$$

where $n_{out}(t)$ is the noise signal after the noise $n_{in}(t)$ passing through the linear system.

When the mixer is applied to the linear system output, we produce

$$\begin{aligned}
 y_m(t) &= s(t) \cdot m(t) \\
 &= \left\{ \frac{A_{out}(t)}{2} \left[e^{j(2\pi a t^2 + 2\pi b t + \theta_{out}(t))} - e^{-j(2\pi a t^2 + 2\pi b t + \theta_{out}(t))} \right] + n_{out}(t) \right\} \\
 &\quad \cdot \left\{ -2e^{j(2\pi \alpha t^2 + 2\pi \beta t + \theta_m)} \right\} \\
 &= -A_{out}(t) e^{j[2\pi(a+\alpha)t^2 + 2\pi(b+\beta)t + (\theta_{out}(t) + \theta_m)]} \\
 &\quad + A_{out}(t) e^{-j[2\pi(a-\alpha)t^2 + 2\pi(b-\beta)t + (\theta_{out}(t) - \theta_m)]} \\
 &\quad - 2n_{out}(t) e^{j(2\pi \alpha t^2 + 2\pi \beta t + \theta_m)}
 \end{aligned} \tag{Equation 3-22}$$

where $y_m(t)$ is the mixed output. This resultant signal can be thought of as the sum of three signals — one with the sum sweep rate, one with the difference sweep rate and the other one with the broadband noise. For the difference signal, the frequency variation carries the magnitude and phase information as a function time. By selecting proper values for the mixer, we can produce carrier frequencies at DC (for the difference signal) and at double sweep rate (for the sum signal).

For example, by selecting $\alpha = a$, $\beta = b$, and $\theta_m = 0$ we can get

$$\begin{aligned}
 y_m(t) &= -A_{out}(t) e^{j[2\pi \cdot 2at^2 + 2\pi \cdot 2bt + \theta_{out}(t)]} \\
 &\quad + A_{out}(t) e^{-j[\theta_{out}(t)]} \\
 &\quad - 2n_{out}(t) e^{j(2\pi \alpha t^2 + 2\pi \beta t)}
 \end{aligned} \tag{Equation 3-23}$$

By applying a low pass filter, the double rate signal can be eliminated, as well as most of the noise (except for signal that entered during the start-up transient of the low pass filter).

Thus, if we ignore the start-up, the following output remains after filtering:

$$s_m(t) = A_{out}(t) e^{-j[\theta_{out}(t)]} \tag{Equation 3-24}$$

Now we can see that the magnitude of the output is the instantaneous magnitude of the measured signal and the phase of the output is the instantaneous phase of the measured signal. Then, we can extract the instantaneous magnitude and phase information of the measured signal in the time domain.

$$A_{out}(t) = |s_m(t)|$$

$$\theta_{out}(t) = -\angle s_m(t)$$

Equation 3-25

3.2.2 System Configuration

The simulation processing for this technique also has two steps:

1. Generate the calibration signal to construct the equalization.
2. Measure the performance by calculating the CMRR at 60 Hz.

The simulation model for equalization filter design is show as Figure 3-11.

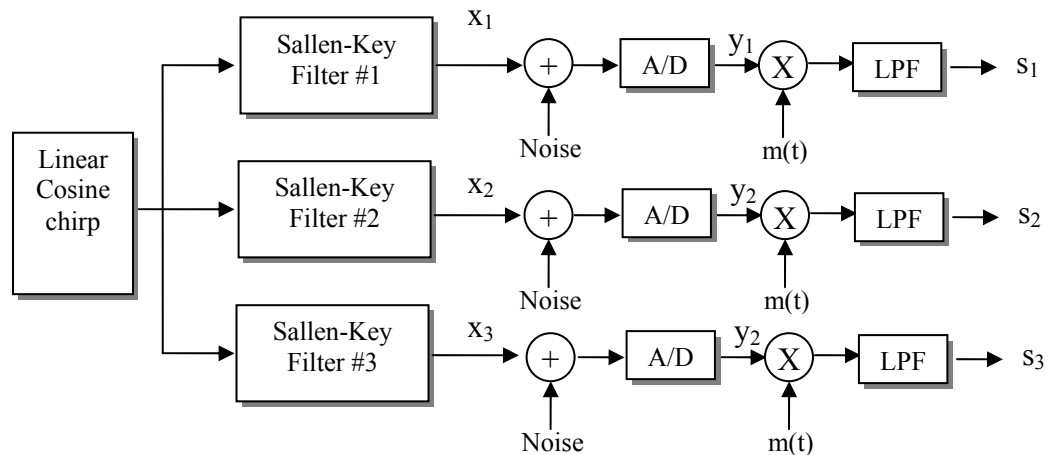


Figure 3-11 Equalization filter design model using mixing technique

To design the equalization filter, the most difficult issue is the design of the low-pass filter (LPF) that resides after the mixer, since its cut-off frequency should be less than 1% of the Nyquist frequency. At first, we attempted to design the LPF in the frequency domain using the optimal nonrecursive digital filter presented by Rabiner in 1970 [Rabiner]. The performance of this filter was not sufficient. Thus, we resorted to a filter designed using the windowing method which utilizes a large number (greater than 3000) of coefficients. The number of filter coefficients is limited by the start frequency

and sweep duration of the input chirp signal. The EMG signal contains most of its power from 50-150Hz. Thus, the length of the LPF must be such that the input chirp, which sweeps upwards from 0 Hz, is not distorted in the 50–150 Hz range due to the startup transient of the filter.

3.2.3 CMRR Measurement

CMRR measurement with the mixing technique was logically the same as using the conventional technique and is re-drawn as Figure 3-12. However, we previously noted that CMRR measurement via the power spectrum is impractical for high CMRR measurement. In order to measure the PSD of the common mode signal, the noise level in the signal cannot be higher than the 60 Hz signal.

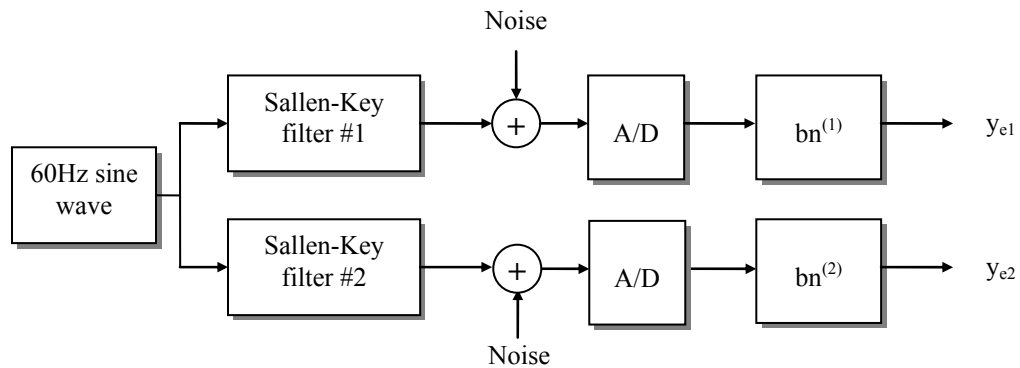


Figure 3-12 CMRR measurement model

Figure 3-13 shows the PSD plots for simulations resulting in low and high CMRRs. The x-axis in this figure is normalized frequency. For the low CMRR case (40 dB), the 60 Hz signal is visible in the PSD plot. In this case, we can estimate the PSD for the common mode signal. While for the high CMRR (90 dB), the 60 Hz signal is unclear because the noise dominates the whole signal. By using the mixing technique, the

expected CMRR is higher than using the conventional technique, thus we cannot use the same method to measure the CMRR. In this section, we describe a method for measuring higher CMRRs and point out the limitation of this method.

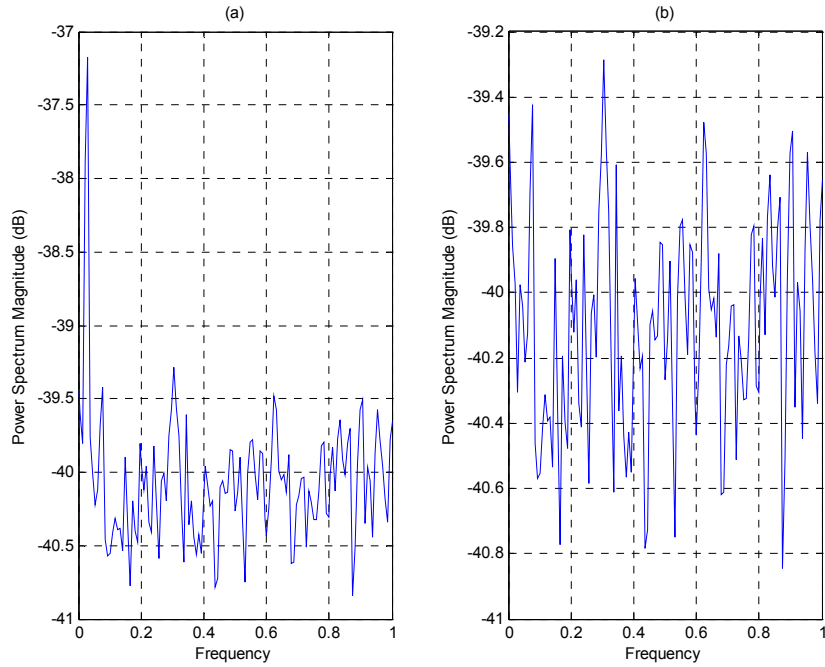


Figure 3-13 PSD plots for different CMRR (a) low CMRR, 40 dB, (b) high CMRR, 60 dB

The CMRR between the two outputs y_{e1} and y_{e2} can be calculated from Equation 3-14.

$$CMRR = 20 \log_{10} \left(\frac{|A_d|}{2 \cdot |A_c|} \right) \quad \text{Equation 3-14}$$

where A_d is the magnitude of the sum of the two signals and A_c is the magnitude of the difference between the two signals. Define $s(t) = y_{e1}(t) + y_{e2}(t)$ and $d(t) = y_{e1}(t) - y_{e2}(t)$. In general, we can use the PSD estimation technique to measure the magnitude of $s(t)$, as the magnitude of this signal is well above the noise floor. To measure the magnitude of $d(t)$, a new method was investigated in simulation.

NSR (noise – to - signal ratio)

We define NSR as a measure of signal strength relative to the background noise. NSR is the ratio of the standard deviation σ_N of the noise to the magnitude Amp_s of the 60 Hz signal, where the noise is white Gaussian noise.

$$NSR = \frac{\sigma_N}{Amp_s} \quad \text{Equation 3-26}$$

From the definition of NSR, the magnitude A_c of $d(t)$ can be written as

$$A_c = \sigma_N / NSR \quad \text{Equation 3-27}$$

Substituting Equation 3-27 into Equation 3-14, we get

$$CMRR = 20 \log_{10} \left(\frac{|NSR \cdot A_d|}{2|\sigma_N|} \right) \quad \text{Equation 3-28}$$

CMRR Measurement

The simulation model is shown in Figure 3-14.

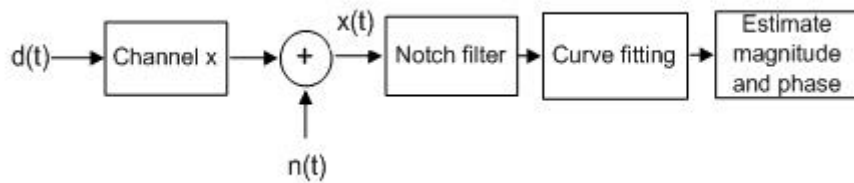


Figure 3-14 CMRR measurement model

where $d(t)$ is the incoming signal, $n(t)$ is additive white Gaussian noise and $x(t)$ is the output of channel x. To simplify this simulation, consider a 60Hz signal $d(t)$ with large additive white Gaussian noise $n(t)$

$$x(t) = d(t) + n(t) \quad \text{Equation 3-29}$$

We focus on the estimate of the magnitude of $d(t)$. Because the noise is white and Gaussian, noise outside of the frequency region around 60 Hz can be attenuated via the use of a notch filter. Letting signal $x(t)$ pass through this notch filter, most of the noise will be eliminated. The output can be written as

$$x_1(t) = d(t) + n_1(t) \quad \text{Equation 3-30}$$

where $n_1(t)$ is the residual noise. To estimate the magnitude of $d(t)$, we use nonlinear curve fitting to fit $x_1(t)$ into a 60 Hz signal $d_{est}(t) = Amp_{est} \sin(2\pi * 60t + \theta_{est})$. The magnitude Amp_{est} of $d_{est}(t)$ is the common signal amplitude.

Here we show some simulation results. In this simulation, we evaluated 10 second, 100 second and 200 second signal durations. For each input signal, we let the 60 Hz input have unit magnitude and we varied the noise to signal ratio (NSR). We used this method to measure the magnitude and phase of the input signal and compared the measured results to the ideal values. We repeated every simulation scenario 1000 times to get 1000 results and computed the sample mean and sample standard deviation of these 1000 results. The results are shown in Figure 3-14 and Figure 3-15.

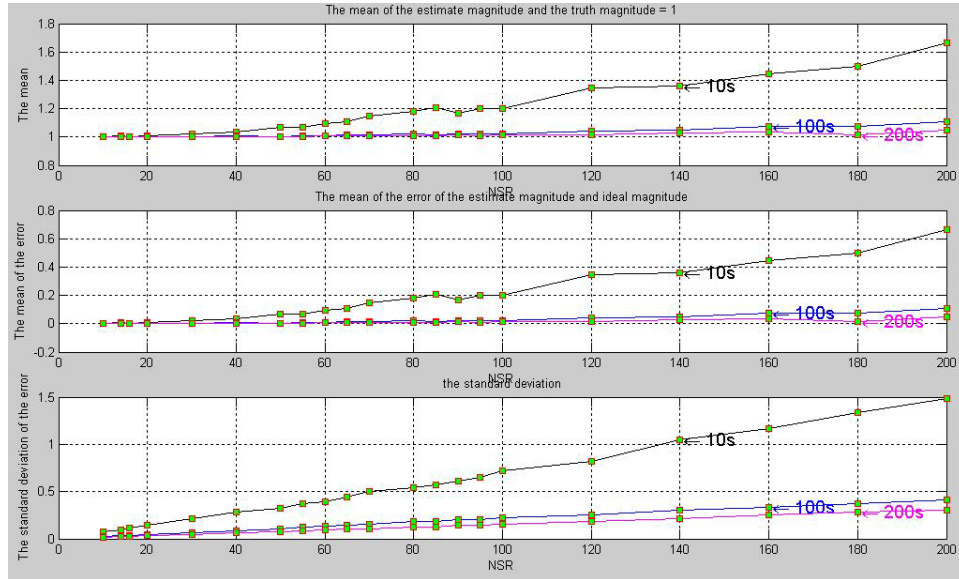


Figure 3-15 The mean and standard deviation of the error between the estimate and ideal magnitude and the mean for the estimate magnitude (ideal magnitude = 1)

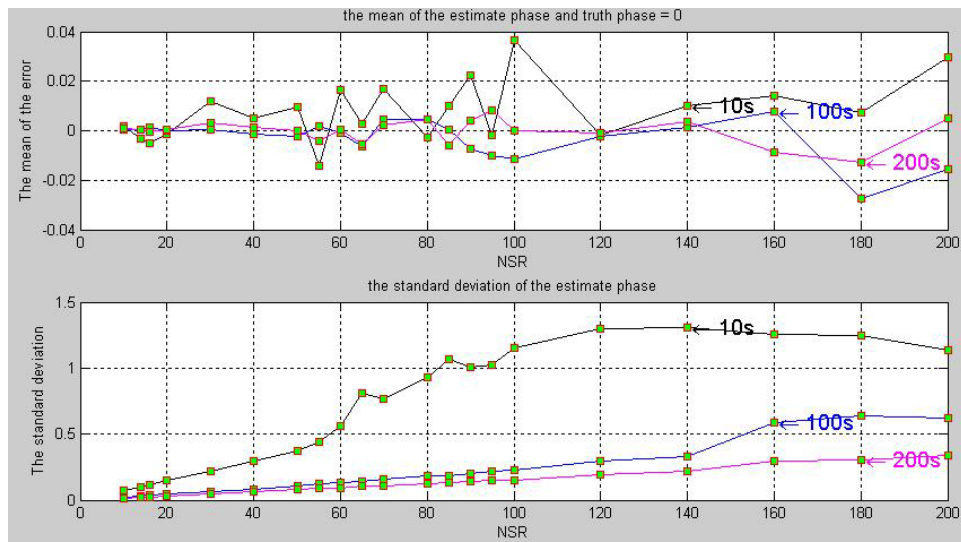


Figure 3-16 The mean and standard deviation of the error of the estimate and ideal phase

Discussion

From the result of the experiments, we can see that for 100 second and 200 second signal durations, even a NSR is large as 100 still resulted in an amplitude estimate with acceptable error. From Equation 3-28

$$CMRR = 20 \log_{10} \left(\frac{|NSR \cdot A_d|}{2|\sigma_N|} \right) \quad \text{Equation 3-28}$$

Letting $NSR = 100$ and $A_d = 2$ $\sigma_N = 0.01$, we can get

$$CMRR = 20 \log_{10} \left[\frac{100 \cdot 2}{2 \cdot 0.02} \right] = 73.9 \text{ dB}$$

Thus, with a 100 second input, we can expect to measure CMRRs up to 73.9 dB if there is 0.1% noise in a 1 volt input signal. In practice, however, this method may measure higher CMRRs for two reasons.

First, the standard deviation of the noise in hardware is not related to the size of the input signal. Thus, the magnitude of the input signal can be made as high as possible. A higher CMRR can then be measured since we have increased A_d . If the magnitude of the incoming 60 Hz signal can be increased to 4.8 V, the CMRR can increase

$$CMRR = 20 \log_{10} \left[\frac{4.8}{1} \right] = 13.6 \text{ dB} \quad \text{Equation 3-31}$$

Second, using better hardware components can reduce the noise level. For example, we compared the noise resulting from two commonly-used amplifiers: the TL084 and AD620 arranged in a monopolar configuration in a prototype array system on the bench-top. In each configuration, the channel inputs were shorted to circuit ground and the total RMS output noise level was measured. Five distinct prototype hardware channels were constructed for each configuration. Each channel was cascaded with a band pass filter

with the frequency range from 18 Hz to 1800 Hz. Recordings were made with a 16-bit A/D converter on a PC. We found that most of the noise is generated from the amplifier because, arranged as a typical biopotential circuit, these “front-end” amplifiers employed a large gain. Plots of the noise measurements are shown in Figure 3-17. We can see that the AD620-based circuit reduced the noise almost in half. If the noise is cut in half, the CMRR can increase by

$$CMRR = 20 \log_{10}[2] = 6 \text{ dB} \quad \text{Equation 3-32}$$

Overall, a higher input signal amplitude and lower noise amplifiers permit CMRR measurement up to approximately 93.5 dB.

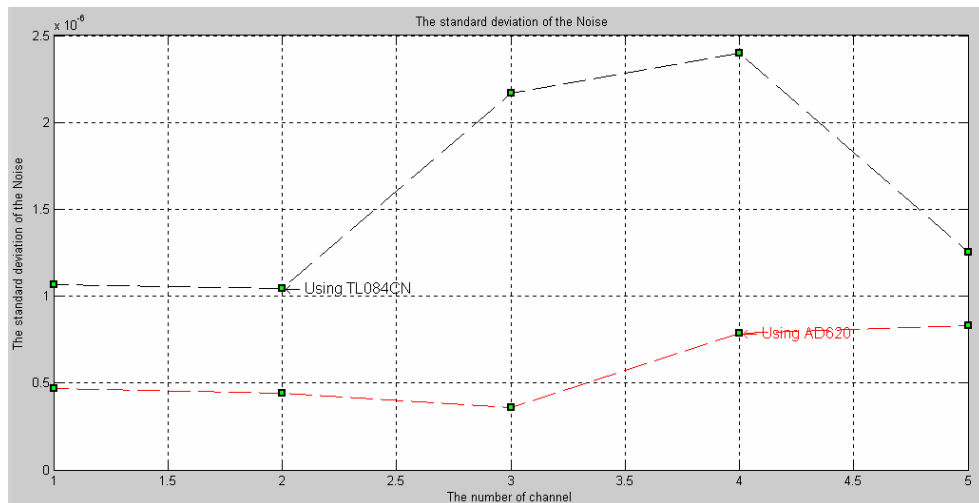


Figure 3-17 The noise generated by two different amplifiers: TL084 and AD620

Additionally, we compared the CMRR that we measured using this method with the true CMRR in a simulation model. The test model is shown in Figure 3-18.

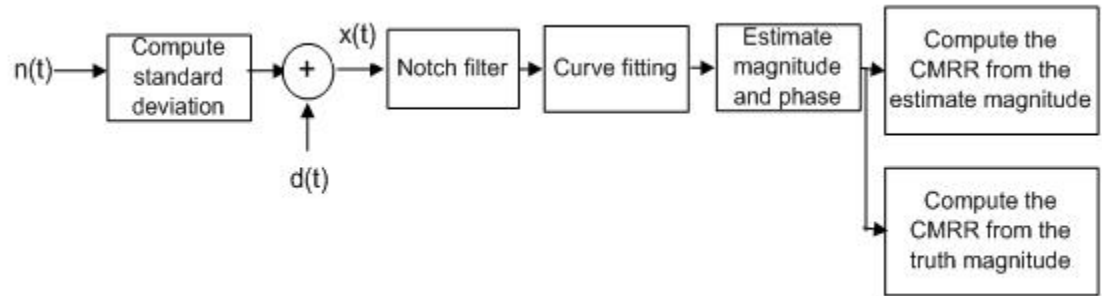


Figure 3-18 CMRR measurement configuration

In this simulation, we replaced the white Gaussian noise with the measured noise from our 5-channel prototype array system. (This prototype system will be presented in more detail in the next chapter.) To perform the simulation, we begin by computing the standard deviation of the noise signal. Then, the 60 Hz signal $d(t)$ for different NSRs was generated from $d(t) = \frac{\sigma_N}{NSR} \cdot \sin(2\pi \cdot 60 \cdot t)$. Using Equation 3-28, the ideal CMRR is computed and compared to the result found by applying our technique to the simulated data. We let the magnitude of both input signals be 4.8 V, hence $A_d = 9.6v$. The simulation results of the ideal vs. computed CMRR for different signal durations are shown in Figure 3-19.

We can see that we can measure CMRR as high as 110 dB. Also, we can see that the estimated CMRR is always less than the true CMRR by approximately 3 dB. The limitation of this technique is that CMRRs greater than 120 dB are difficult to measure.

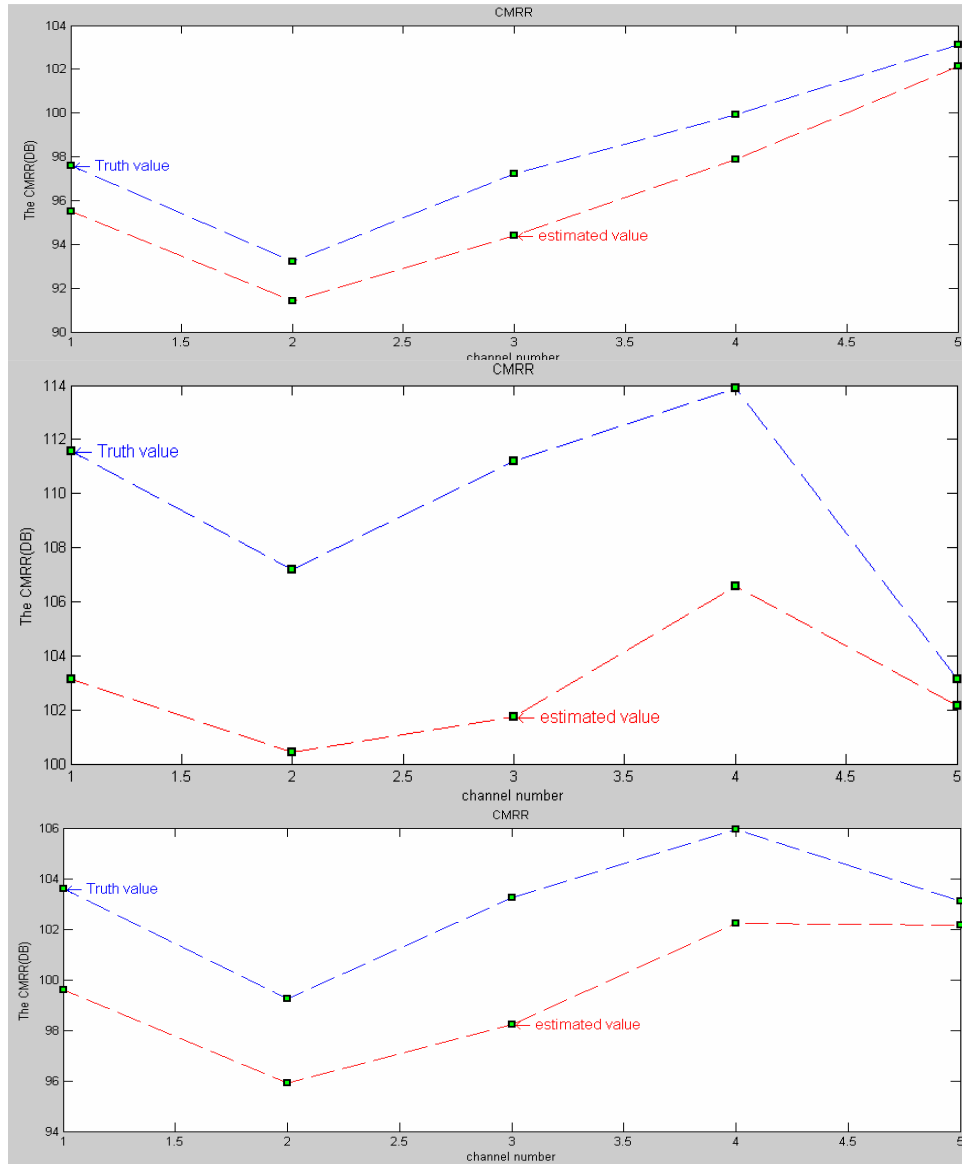


Figure 3-19 Estimated CMRR and true CMRR

In the plots, the lower line is the estimated CMRR and the upper line is the ideal CMRR. Since the data are simulated, the ideal CMRR can be calculated. Compared to the ideal CMRR, the estimated CMRR is always lower than the ideal CMRR.

3.2.4 Simulation Results Using Mixing Technique

In this section, the CMRR results are compared for different equalization filter design techniques. The three major comparisons utilized:

- No software equalization,
- Equalization filter implemented with the conventional technique,
- Equalization filter implemented using the mixing technique.

Using linear shift technique to design the equalization filter in time domain

In this simulation, the noise level is 2 percent. The equalization filter is designed by using the linear shift technique after the frequency response of the equalization filter is determined. For each simulation, CMRR is calculated vs. the length of the FIR equalization filter. The figure shows that using software equalization can improve the CMRR significantly. With the mixing technique, the CMRR can be as high as 75 dB.

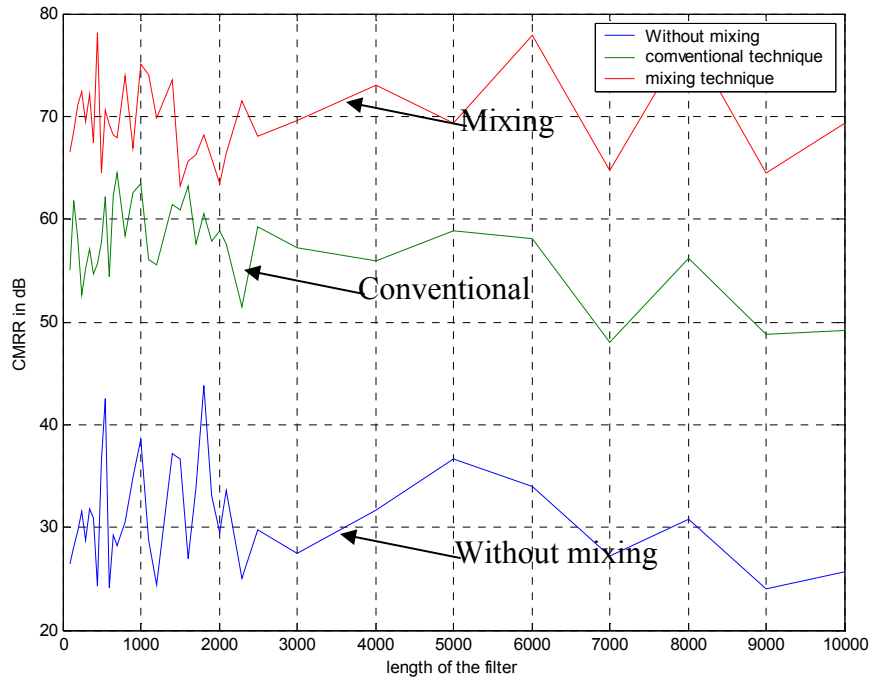


Figure 3-20 CMRR using linear shift technique

Using windowing technique to design the equalization filter in time domain

The next simulation is performed using the same conditions as above, except that the equalization filter is designed using the simple windowing technique (i.e., absent the linear shift). The figure also shows that using software equalization filter can improve the CMRR and that the mixing technique achieves the highest CMRRs. When equalization is performed, the linear shift operation produces superior equalization filters.

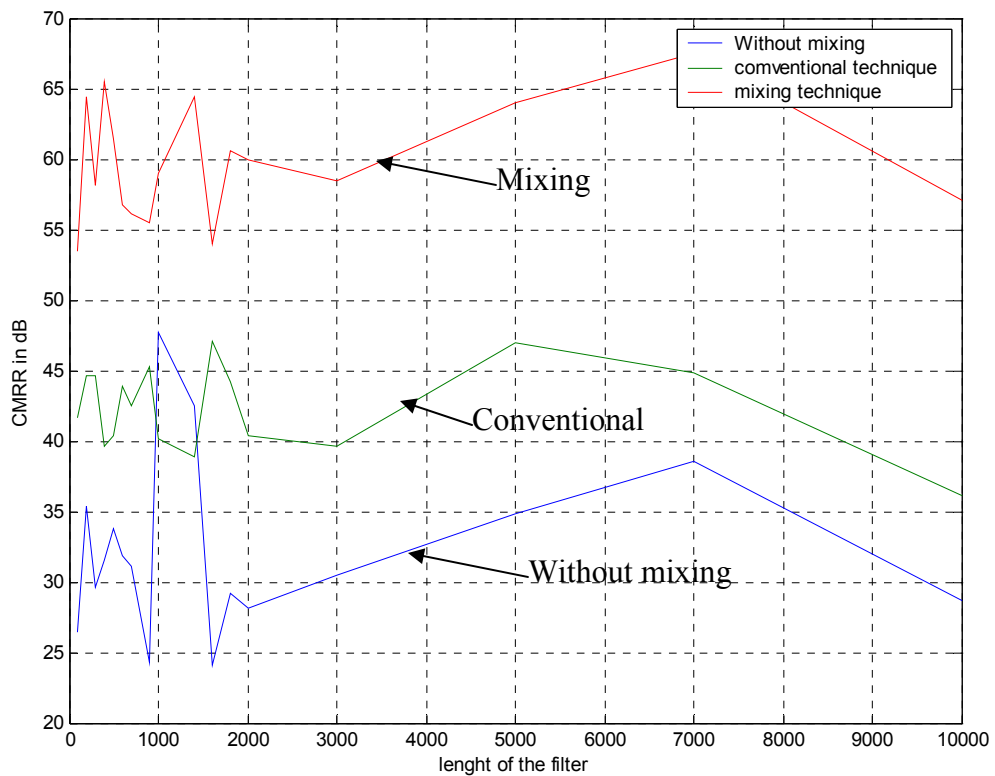


Figure 3-21 CMRR using windowing technique

CHAPTER 4 LABORATORY EXPERIMENTS

4.1 *Hardware Introduction*

All the laboratory data described above are recorded from a five-channel prototype system. Each channel consists, in sequence, of four stages:

- Stage 1: Eighth order, unit gain, Sallen-Key, Butterworth filter with cut-off frequency at 15 Hz. This stage attenuates motion artifact during severe movement conditions.
- Stage 2: Selectable gain: There are eight selectable values. The gain prior to the first high-pass filter stage is 10. Gain selection resolution is a factor of two per step. Since the electrode-amplifier circuit is designed for a gain of 100, the signal conditioning circuit's gain can range from 5–200. The different gain selections must be discrete in order to be reproducible for use in channel equalization. The available set of gain selections is: 2, 4, 8, 16, 32, 64, 128 and 256.
- Stage 3: Electrical isolation: Provided by a unity-gain circuit accepting inputs over the range of ± 5 V.
- Stage 4: Low-pass filter: Fourth-order, unity-gain, Sallen-Key, Butterworth design with cut-off frequency at 1800 Hz.

The schematic of the circuits used in this project can be found in the appendix. In this project, a Matlab program (`capture_data.m` [*Mark*]) is used to record the data via the PC and A/D converter board.

In any hardware system, the most important issue is the inevitable presence of broadband background noise in the calibration signal. Before any calibration data are recorded, the noise level is measured for our prototype system by grounding the input of

each channel. Here we only test the first three channels because we only need three channels to test the performance of the mixing technique. After several experiments, the measured noise standard deviation is shown in Table 4-1. Because the EMG signal ranges from 15 to 500 Hz and the cut-off of the high pass filter stage is 15 Hz, we also measured the noise standard deviation over the frequency band from 15 to 500 Hz. From the results, we can see that the total noise standard deviation is typically 0.5~0.7 μv , which is similar to amplifier circuits described in the EMG literature. For each experiment, by grounding the input, the output signal was recorded at the same condition. All the experiments are done at the same day. The first three are done in the morning while the last two are done in the afternoon.

Table 4-1 Measured Noise standard deviation (in μv)

		Channel I	Channel II	Channel III
Experiment I	Noise (whole bandwidth)	0.558	0.612	0.627
	Noise (15~500Hz)	0.301	0.305	0.302
Experiment II	Noise (whole bandwidth)	0.814	0.864	0.874
	Noise (15~500Hz)	0.314	0.367	0.373
Experiment III	Noise (whole bandwidth)	0.621	0.658	0.645
	Noise (15~500Hz)	0.321	0.314	0.313
Experiment V	Noise (whole bandwidth)	0.58	0.626	0.677
	Noise (15~500Hz)	0.291	0.291	0.291
Experiment IV	Noise (whole bandwidth)	0.55	0.585	0.627
	Noise (15~500Hz)	0.291	0.294	0.302

For each calibration data recording, a linear chirp signal which is generated from a signal generator propagates through the five distinct hardware channels and is recorded in Matlab via the A/D converter. For every experiment, the chirp signal frequency ranges from 0 to 2 K Hz and is 100 seconds in duration. As we discussed in chapter 3, in order to generate the mixer, we need to estimate the frequency sweep rate and the initial

frequency for the original chirp signal, so the signal from the generator is also recorded to provide the necessary information. Hence for each recording, there are six channels of data presented. The first five channels are from the respective hardware channels and the sixth channel is a direct sampling of the signal generator output. Because the start time of the chirp signal can not be perfectly synchronized, we allotted additional recording time beyond the desired recording duration. This additional recording “buffer” is removed prior to any signal processing.

The voltage range of our A/D converter is $\pm 5V$. Our prototype system has a minimum gain of 10 and a maximum gain of 2560. Thus, the maximum voltage of the input is $5v / 2560 = 1.95mv$, while the minimum voltage that the signal generator can produce is 50 mV. Therefore, the interface between the signal generator and the input of the system is not directly connected. To satisfy the voltage requirement, the output of the signal generator was passed through a two-resistor voltage divider circuit, and from there into the prototype system.

The data are saved into a .daq file in the Matlab format. The sampling rate is always 4096 samples/second. The recording apparatus are arranged as shown in Figure 4-1.

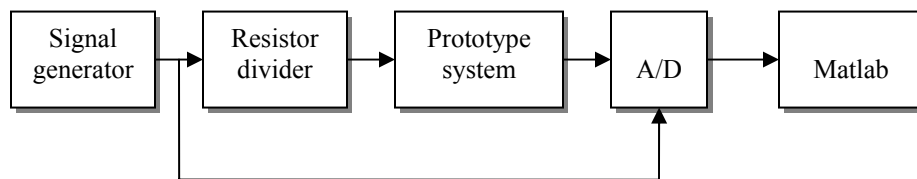


Figure 4-1 Recording processing model

Figure 4-2 shows an example of the six acquired channels using a 100 second recording duration plus a 5 second buffer time. Figure 4-3 shows the calibration data after the

buffer period is removed. In this project, the buffer period was manually identified for each recording.

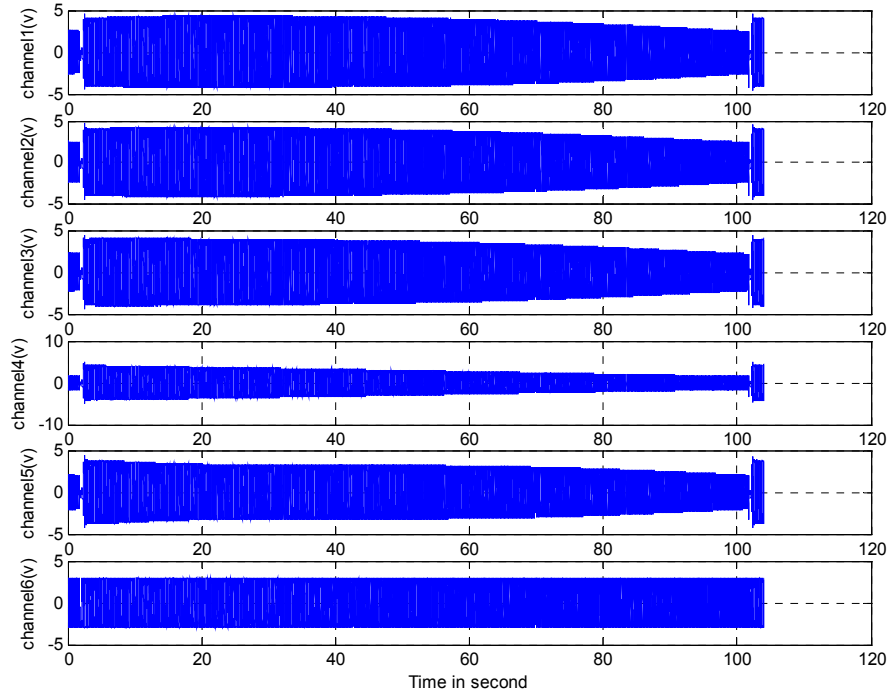


Figure 4-2 Calibration data

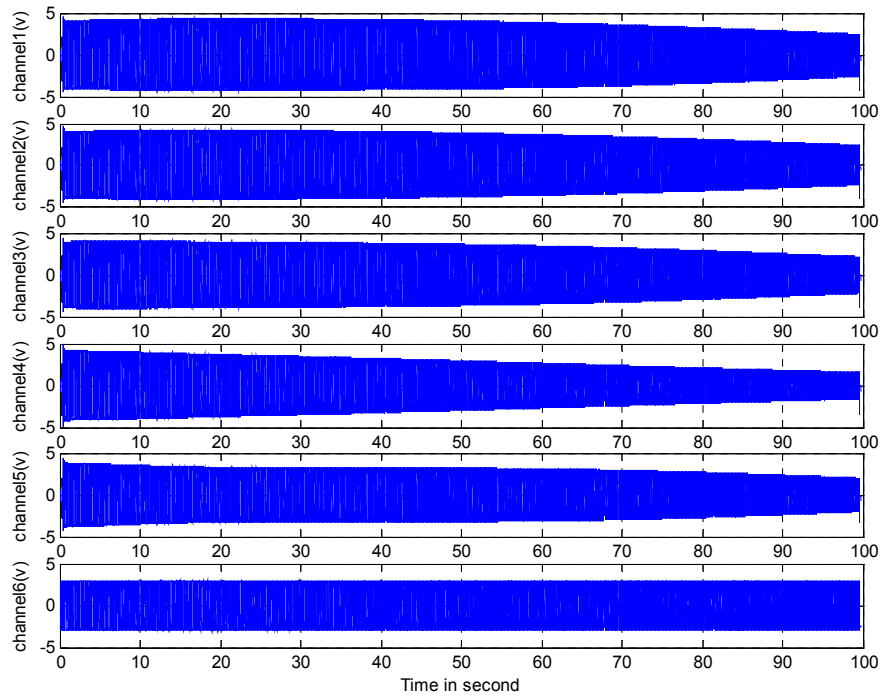


Figure 4-3 Calibration data after carving out the buffer

The equalization filter design configuration is shown as Figure 4-4.

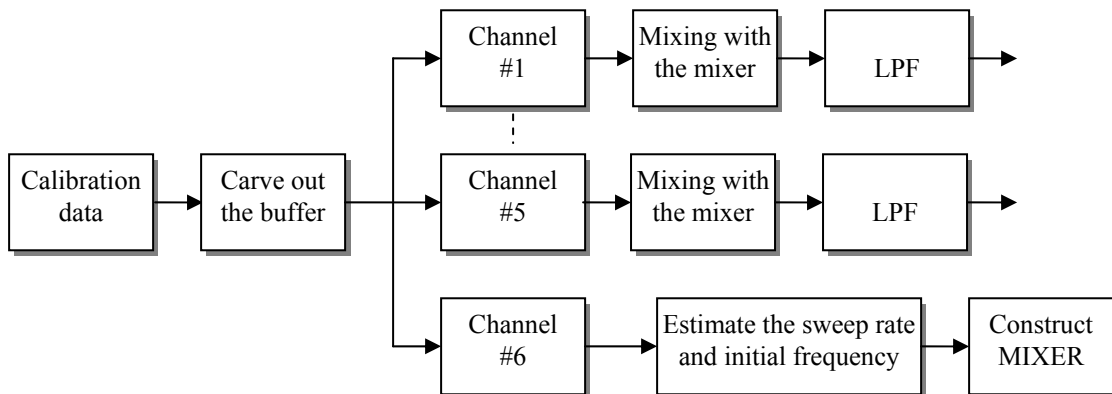


Figure 4-4 Configuration for equalization filter design

Note that the sixth channel that directly comes from the signal generator was used to estimate the sweep rate, initial frequency and the phase. They were estimated using a

nonlinear least squares fit to a prototype chirp (Matlab optimization toolbox). A precise initial guess should be given when using this method.

4.2 Experiment Results

In this section, we compare the results between using the conventional technique and the mixing technique. The data used in this analysis were recorded on July 11, 2004 (file name: “ch0711.daq”).

4.2.1 Equalization Filter Response

In this analysis, we implemented the equalization filter using the linear shift technique. Figure 4-5 shows the magnitude response of the filter in the frequency domain and its zoomed view. In the plot, the blue color presents the equalization filter from the conventional technique and the red color presents the equalization filter from the mixing technique. In this plot, we can see that there are some distortions at the beginning and the end of the filter because of the start transient. Since the dominant energy of the EMG signal is in the range of 15-150Hz, the start transient is ignored.

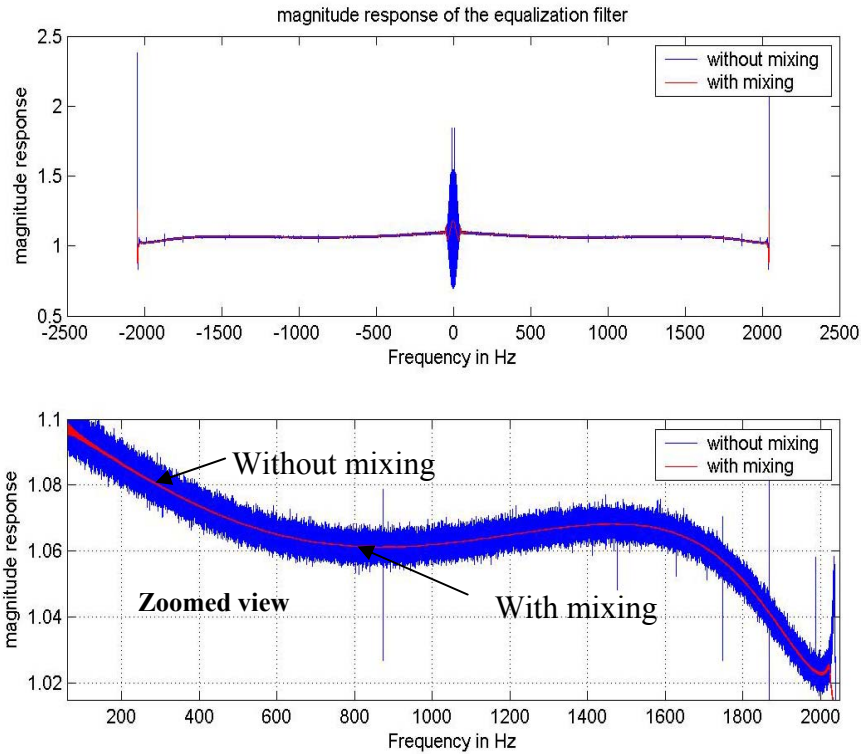


Figure 4-5 Magnitude response of the equalization filter

4.2.2 CMRR Results

In this section, we only show the results using the linear shift technique. The calibration data named “ch0711.daq” is used to design the equalization filter using linear shift technique. Two 60 Hz sine wave signal named “sin0711.daq” and “sin0712.daq” are used to evaluate the equalization filter. Each recording has 100 seconds duration. Since it is five channel prototype, each 60 Hz sine wave can be perform several bipolar configuration. The CMMR is the mean value of all the bipolar configuration.

	Conventional technique	Mixing technique
CMRR	35dB	72dB

CHAPTER 5 PRELIMINARY RESULTS From A 28- CHANNEL ELECTRODE ARRAY

5.1 *EMG hardware system*

5.1.1 The EMG Array

In this project, a 28-channel electrode array is also used to recode the EMG signal. In this section, the preliminary results using the mixing technique with this array will be described. The array was constructed as a 4x7 rectangular grid. Each electrode consisted of a stainless steel M2 screw arranged 5 mm center to center from adjacent electrodes. Each electrode was connected to a gain of 20, high-impedance differential amplifier (Analog Devices AD620 Instrumentation Amplifier). To achieve a monopolar configuration, the second input to each differential amplifier was from a common monopolar reference electrode. An additional electrode served as the isolated power supply reference. These additional electrode contacts were also stainless steel. The electrodes and amplifiers were mounted on a printed circuit board (PCB) which was epoxy encapsulated. Flexible wiring cables connected this pre-amplifier to the signal conditioning apparatus.

A one layer PCB board is designed. There are 14 channels on each side. Figure 5-1 shows the schematic of the top of the array PCB board and Figure 5-1 shows the completed electrode array used in this project.

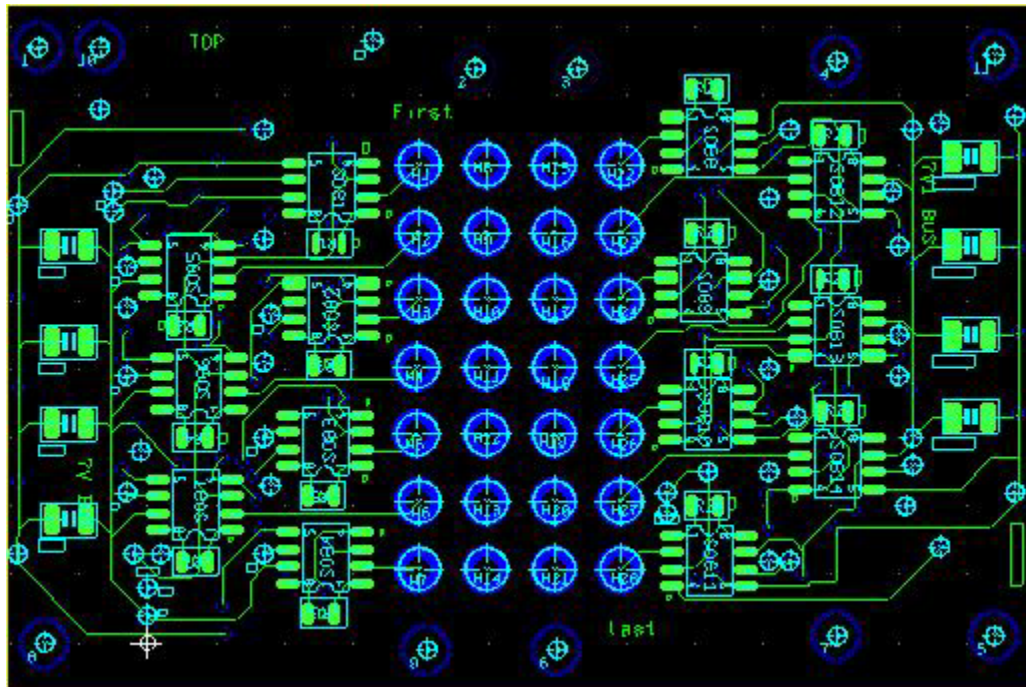


Figure 5-1 The schematic of one side of the array PCB board

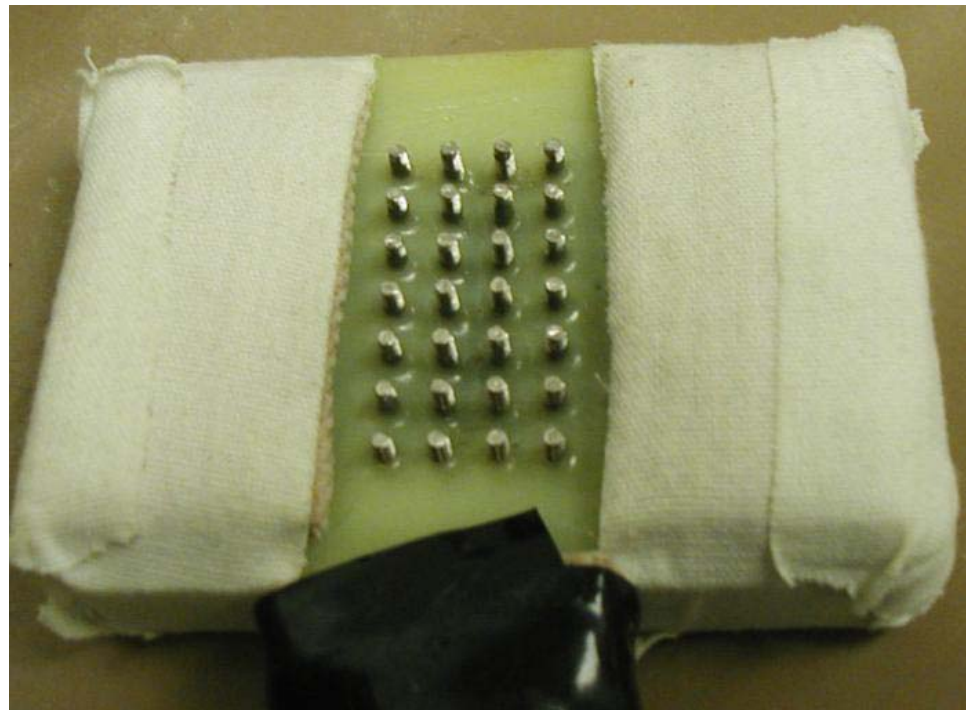


Figure 5-2 The electrode array

5.1.2 Signal Conditional Circuits

The design of the signal conditioning circuits is identical to the circuits presented in chapter 4. In this research, four conditioning circuits were built into one signal conditioning unit via a PCB implementation of the circuit design. All units were powered from two power supplies, one of which maintained electrical isolation from earth ground.

5.2 Experiment Results

Prior to each experiment, conductive electrical gel is applied to the electrode and the skin to reduce the electrode-skin impedance. Each EMG recording is 5 seconds long and the calibration data are 100 seconds long (plus the buffer duration). Figure 5-3 shows a sample EMG recording from our 28-channel array. The x-axis is the time vector in seconds and y-axis is the magnitude of the EMG signal. Figure 5-4 and Figure 5-5 show that equalized EMG signal of one channel with bipolar and NDD configuration. Figure 5-6 and Figure 5-7 show one of the channels with NDD spatial filter before and after equalization. The plots show that with equalization, the MU can be easily identified.



Figure 5-3 28 channels EMG signal review

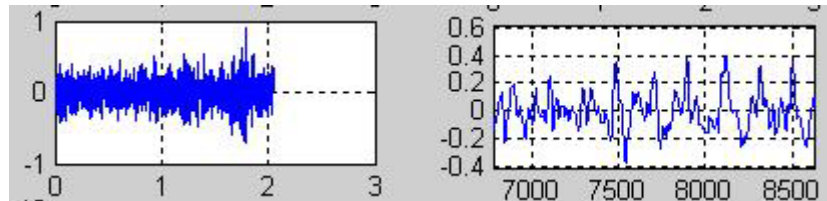


Figure 5-4 Equalized EMG signal (Bipolar) Right side is the zoomed view

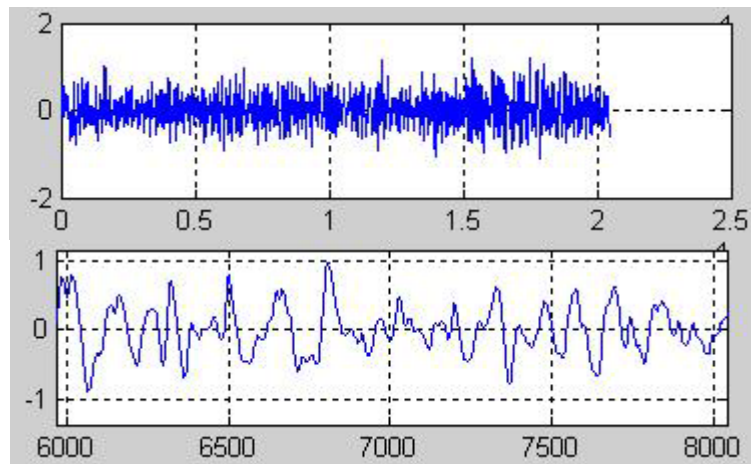


Figure 5-5 Equalized EMG signal (NDD) Lower is the zoomed view

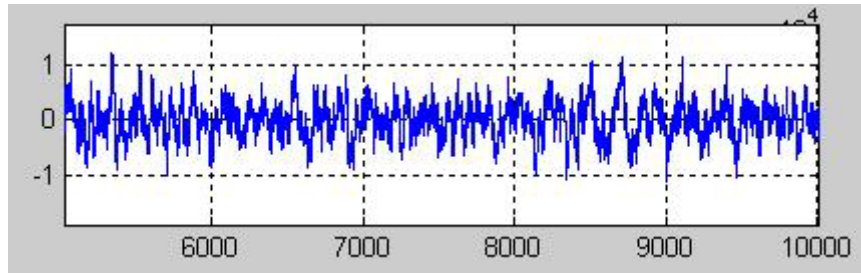


Figure 5-6 EMG signal (NDD) before equalized

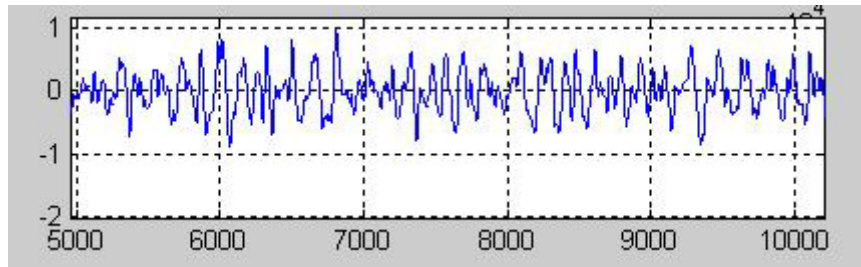


Figure 5-7 EMG signal (NDD) after equalized

CHAPTER 6 CONCLUSIONS AND FUTURE WORK

6.1 Discussion

In this section, we briefly summarize the conclusions drawn from this project. In recent years, there has been increasing interest in detecting single MU activity via noninvasive spatial filtering techniques. In general, the spatial filtering is implemented in hardware. Due to the limitations in hardware, we sought to achieve high-quality, flexible spatial filtering using software channel equalization. We explored different techniques to design the equalization filter. Our conventional technique consisted of taking the ideal frequency response divided by the measured frequency response to determine the frequency response of the equalization filter. We showed that conventional channel equalization can improve the CMRR, but not sufficiently so and it is very sensitive to noise.

Since the major problem is broadband background noise, it became necessary to eliminate as much noise as possible before implementing the equalization filter. Thus, we pursued de-noising via a mixing technique. This new technique is evaluated with both simulation and laboratory experiments. From the results shown in chapter 3 and chapter 4, it is clearly observed that the mixing technique can improve CMRR more than the conventional technique and it is much less sensitive to noise. In this project, we are typically achieving a CMRR of 64-85 dB at 60 Hz after mixing and equalization, but less than 40 dB with conventional equalization.

6.2 Future Work

First, based on the previous discussion, the premise of our software mixing technique has been demonstrated. The mixer requires the initial frequency of the excitation chirp and its sweep rate. We found our results to be sensitive to the accuracy of determining these parameters via an optimization algorithm. In the future, we can either use a new algorithm to estimate them, or produce a better initial guess when using the Matlab optimization toolbox.

Second, to eliminate the noise, we can consider using a linear time-varying band-pass filter (LTV). By using this technique, there exists a trade-off between the amount of noise reduction and the amount of signal distortion. Preliminary simulations for testing the noise reduction performance of LTV filters suggested that a smaller passband reduced most of the noise, but caused large signal distortion. High-order LTV filters can significantly improve these issues, but might result in an unacceptable start up transient. But, we could alternatively use a low-order LTV filter cascaded with our mixing technique. In the future, we can measure the performance via the use of LTV filters together with our mixing technique.

Third, the most difficult challenge in the mixing technique is the low pass filter design stage, since the cut-off frequency of the low pass filter must be set to less than 1% of the Nyquist frequency. Currently the order of the low pass filter is greater than 3000. In the future, we may investigate a better technique to design the low pass filter.

Fourth, we find that the achieved CMRR is much better if the calibration data duration is longer. Currently, we are using a 100 second chirp signal to calibrate the equalization filter. By using longer duration data recordings with a slower frequency

ramp, we can use larger order low-pass filters after the mixer to eliminate more noise (because a longer filter startup transient can be tolerated). Another possible solution is to use two 50 second duration chirps instead of one 100 second duration chirp. The first chirp could ramp in frequency from 0 to 500 Hz and the other one from 500 to 2 KHz. Their resulting transfer function could be assembled in the frequency domain to provide information over the complete frequency range. Finally, we might consider upsampling the signal prior to the mixing stage to determine if low-pass filters implemented at the upsampled rate can reduce the effective startup transient duration.

REFERENCES

[Clancy01] Edward A. Clancy, Hongfang Xia and Mark V. Bertolina, "A Preliminary Report on the Use of Equalization Filters to Derive High Spatial Resolution Electrode Array Montages," *Proceedings of the International Symposium on Neuromuscular Assessment in the Elderly Worker (NEW)*, Torino, Italy, pp. 103–106, February 20–21, 2004.

[DeLuca79] Carlo J. De Luca, Physiology and Mathematics of Myoelectric Signals. *IEEE Transactions on Biomedical Engineering*, Vol. BME-26, NO. 6, June 1979.

[DeLuca02] Carlo J. De Luca. Surface Electromyography: Detection and Recording. 2002 by DelSys Incorporated.

[Disselhorst97] Catherine Disselhorst-Klug, Jiri Silny, and Gunter Rau, Improvement of Spatial Resolution in Surface-EMG: A Theoretical and Experimental Comparison of Different Spatial Filters. *IEEE Trans. Biomed. Eng.*, Vol. 44, No. 7, July 1997.

[Disselhort98] Catherine Disselhort-Klug, Gunter Rau, Astrid Schmeer, Jiri Silney. Non-invasive detection of the single motor unit action potential by averaging the spatial potential distribution triggered on a spatially filtered motor unit action potential. *Journal of Electromyography and kinesiology* 9(1999) 67-72.

[Hambley] Allen Hambley. Electronic 2nd Edition. *Prentice Hall* 1999.

[Mark] Mark V. Bertolina, Khoi Le, Hai Trinh. Active Power-Line Interface Attenuation in Bioamplifiers. *Project Number: EXC-0201-EE*.

[Met90] A. C. MettingVanRijn, A. Peper, C. A. Grimbergen. High Quality Recording of Bioelectric Events. I: Interference Reduction, Theory and Practice. *IEEE Medical & Biological Engineering & Computing*, vol. 28 pp. 389-394, <http://www.biosemi.com/publications/artikel3.htm>, Sept. 1990.

[Neuman] Neuman, MR. Biopotential Electrodes. *The biomedical Engineering Handbook, Second Edition* 48: 1-12.

[Proakis96] John G. Proakis, Dimitris G. Manolakis, Digital Signal Processing Principles, Algorithms, and Applications 3rd Edition. *Prentice Hall ISBN 0-13-373762-4*.

[Rabiner] Lawrence R. Rabiner, Bernard Gold and C. A. McGonegal. An Approach to the Approximation Problem for Nonrecursive Digital Filters. *IEEE Transactions on Audio and Electroacoustics. Vol. AU-18, No. 2 June 1970*.

[Rau97] G. Rau and C. Disselhorst-klug. Principles of High-Spatial-Resolution Surface EMG (HSR-EMG): Single Motor Unit Detection and Application in the Diagnosis of Neuromuscular Disorders. *J. Electromyogr. Kinesiol. Vol. 7, No. 4, pp. 233-239, 1997*.

[Reucher86] Rau G, Reucher H, Schneider J, Silny J. Design and application of spatially filtering EMG electrode configurations. *In: Proceedings of Eighth Annual Conference of the Engineering in Medicine and Biology Society. Fort Worth, 1986:522-5*.

[Reucher87] H. Reucher, G Rau, and J. Silny. Spatial Filtering of Noninvasive Multielectrode EMG: part I-Introduction to Measuring Technique and Applications. *IEEE Trans. Biomed. Eng., vol. BME-34, No. 2, pp98-105, 1987*.

[Reucher87b] H. Reucher, J. Silny and G. Rau. Spatial Filtering of Noninvasive Multielectrode EMG: Part II-Filter Performance in Theory and Modeling. *IEEE Trans. Biomed. Eng.*, vol. BME-34, No. 2, pp106-113, 1987.

[Scott] Dr. Scott Day. Important Factors in Surface EMG Measurement. *Bortec Biomedical Ltd.* 225, 604-1st ST SW Calgary, AB T2P 1M7. www.bortec.ca.

[Stalberg80] Stalberg E, Antoni L. Electrophysiological cross section of the motor unit. *J Neurol Neurosurg Psychiatry* 1980; 43:469-74.

[Texas] Texas Instruments, Analysis of the Sallen-Key Architecture Application Report. *July 1999 – revised September 2002.*

[Webster73] James C. Huhta and John G. Webster. 60-Hz Interference in Electrocardiography. *IEEE Transactions on Biomedical Engineering*, Vol. BME-20, No. 2, March 1973.

[Webster83] Winter, Bruce B., Webster, John G. Driven-Right-Leg Circuit Design. *IEEE Trans, Biomed. Eng.*, Vol. BME-30 pp. 62-66, January 1983.

[Webster99] Webster, John G. The measurement, Instrumentation, and Sensors Handbook. *Sec. 74.* 1999.

APPENDIX Signal Conditioning Circuit Schematics

